International Journal of Biological Macromolecules 329 (2025) 147712

Contents lists available at ScienceDirect

International Journal of Biological Macromolecules

journal homepage: www.elsevier.com/locate/ijbiomac

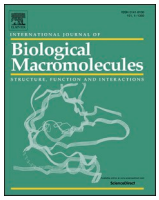

Temperature and time induced assembly phase changes of engineered spidroin protein solutions

Dmitry Tolmachev [a,c], Isabell Tunn [b,c,d], Adam L. Harmat [a,c], Nea B. Möttönen [b,c], Alberto Scacchi [b,c,e], Markus B. Linder [b,c], Maria Sammalkorpi [a,c,*]

[a] Department of Chemistry and Materials Science, Aalto University, P.O. Box 16100, FI-00076, Aalto, Finland
[b] Department of Bioproducts and Biosystems, Aalto University, P.O. Box 16100, FI-00076, Aalto, Finland
[c] Academy of Finland Center of Excellence in Life-Inspired Hybrid Materials (LIBER), Aalto University, P.O. Box 16100, FI-00076, Aalto, Finland
[d] Fraunhofer Institute for Applied Polymer Research (IAP), Geiselbergstraße 69, 14476, Potsdam, Germany
[e] Department of Mechanical and Materials Engineering, University of Turku, Vesilinnantie 5, FI-20014, Turku, Finland

ARTICLE INFO

Keywords:
Spidroins
Silk-like proteins
Temperature response
Liquid-liquid phase separation
Gelling

ABSTRACT

Here, we explore the molecular level origins of the curious temperature and time dependent assembly phase response of silk-like protein materials. Combining molecular dynamics simulations, CD and FTIR spectroscopy, as well as optical microscopy, we examine the assembly phase response of model engineered tri-block protein constructs with a middle intrinsically disordered region and folded terminal domains. We show that, the assembly phase response over a broad temperature range between 20 and 80 °C arises from strong interprotein interactions. The phase transitions are governed by the interplay of changes in the entropy of the flexible glycine-rich regions and the hydrophobic interactions between the α-helices rich in alanine (Ala). Furthermore, we observe irreversible gelation at high temperatures and during aging (time-induced gelation). Thermal gelation rises via interactions between the Ala-rich regions and subsequent formation of β-sheets that crosslink the protein network. On the other hand, the time-induced gel is formed with no notable secondary structure transitions of the middle block via percolation of the protein, which is sensitive to the dimerizing interactions of the terminal domains. Overall, the significance of this work is that we identify time as a separate design variable from the molecular level characteristics and solution conditions of the silk-like protein gels, and extract assembly guidelines for the gel formation and its characteristics.

1. Introduction

Propelled by bioinspiration and the emerging prospects of biosynthetic production approaches, protein-based materials hold immense possibilities in biomaterials solutions for advanced materials [1–3]. Specifically, silk-like proteins offer fascinating materials solutions, e.g., tissue engineering, wound dressings, drug delivery, intelligent health monitoring, food packaging, and textile industry [4–6]. Besides advanced solutions for static, traditional materials characteristics, these protein-based materials also show great promise in dynamically rearranging and adaptive materials [7–9]. The diversity of available applications emerges from the exceptional mechanical properties [10], biocompatibility [11,12], biodegradability [13,14], and high thermal conductivity [15], but also the intrinsically disordered, multi-conformational assembly of the proteins [16,17]. Additional appeal of silk-like materials stem from the possibility to tailor the material properties through precise control of the amino acid sequence and the multiscale assembly structure of the protein material.

Significant interest in silk-like proteins for materials solutions has focused on spidroins, silk proteins produced by spiders [18,19]. Spidroins have a tri-block structure where an intrinsically disordered region (IDR) is terminated by two folded domains [18]. The IDR has a structure of alternating hydrophilic disordered glycine-rich regions and hydrophobic alanine (Ala)-rich regions which form α-helices in solution and β-sheets in fibers [18].

The interactions between the terminal domains of silk-like proteins enable governing the structure and properties of protein materials [20]. For example, simple temperature treatment leads to structural changes in silk protein-based materials, including significant changes in their hydrophobicity and mechanical properties [21,22]. The complex

* Corresponding author at: Department of Chemistry and Materials Science, Aalto University, P.O. Box 16100, FI-00076, Aalto, Finland.
E-mail address: maria.sammalkorpi@aalto.fi (M. Sammalkorpi).

https://doi.org/10.1016/j.ijbiomac.2025.147712
Received 30 May 2025; Received in revised form 4 September 2025; Accepted 15 September 2025
Available online 16 September 2025

interprotein interactions inherent to protein systems can make the material structure, assembly dynamics, and the resulting properties sensitive to the processing pathway [23]. This is evidenced also by silk-like protein phase response presenting metastable and sample history dependent properties [24]. The processing dependency also offers advanced tunability of the material. At the same time, processing dependency requires comprehensive understanding of both the thermodynamic and kinetic assembly phase responses of the protein system. Furthermore, amino acid sequence and solution conditions specificity can be expected, complicating further using the time-temperature dependencies in engineering assembly response.

Addressing this, key relations between structure and phase behavior of proteins have been resolved [25–29]. General level overview of the thermodynamics and kinetics of protein solutions follows from considering solutions of folded proteins, which effectively follow colloidal theory [30]. However, IDRs in the protein can radically change both thermodynamic and kinetic assembly response from the colloidal response of folded proteins [20]. This is not surprising, as IDRs enable a high variety of conformations which makes the assembly free energy landscape and transitions more intricate. The increased complexity results in more time and processing pathway dependent assemblies, for example kinetically arrested states, such as gels. To understand the assembly response in the presence of IDRs, one simplifying consideration is that depending on its structure and length, the IDR can be considered to be a block-copolymer that forms diverse structures [31]. Furthermore, the time dependent solution response of a multidomain protein with both IDRs and folded domains strongly depends on the protein structure and interprotein interactions [29,32]. Simplified models of polymer physics aid in generalizing the assembly dependencies. For example, the Flory-Huggins theory [33,34] predicts that an increase in the polymer length leads to an increase of upper critical solution temperature (UCST) of liquid-liquid phase separation (LLPS), and intrinsically disordered proteins (IDPs) also follow this [35].

Besides length, also temperature is a key control parameter in the LLPS of silk-like protein solutions. Depending on the amino acid composition, IDPs can have an UCST (LLPS induced by a temperature decrease), a lower critical solution temperature (LCST) (LLPS induced by a temperature increase), or different combinations of these [28]. For example, glycine rich IDP sequence makes UCST more likely due to the flexibility of glycine promoting significant changes in entropy when temperature decreases [28]. In contrast, hydrophobic amino acids can lead to the appearance of LCST, since hydrophobic interactions become stronger with rising temperature [35–38]. Generally, stronger interprotein interactions promote forming solid-like states, such as gels [36–39].

Also, the amino acid content and their specific sequence influence the kinetic and thermodynamic response of silk-like proteins. For example, Rekhi et al. [37] have shown that distributing multiple weak interaction “stickers” along the protein chain favors LLPS [37]. In contrast, sparsely distributed strong interaction “stickers” more likely result in aggregation and gelling of IDPs. Harmon et al. [36] demonstrated that the gel-liquid transition undergoes a drastic change when the amino acid sequence of multivalent IDPs was altered. A high density of attractive interaction sites (“stickers”) led to gel formation occurring uniformly at elevated protein concentrations. Opposed to this, “stickers” sparsely distributed along the protein chain at relatively low concentrations drove gelation by the increase of local protein concentration due to phase separation [36].

The IDR interactions both with IDRs and folded domains are essential for the kinetic and thermodynamic assembly response of multidomain proteins. We examine this here using a model silk-like spidroin tri-block protein system. The engineered spidroin AQ12 [40] (also called eADF3) protein with two different types of folded terminal domains, cellulose binding module (CBM) [41] and fibronectin type 3 module 10 (FN) [42], is chosen as the focus model protein system. The phase behavior and properties of AQ12-based protein systems and the influence of amino acid sequence on it have been studied previously both in experiment [20,43–48] and in simulations [49–51], which makes it an ideal model system to study. Specifically, we have previously shown the important role of interactions between the folded terminal domains in driving LLPS propensity on a related tri-block silk-like protein system [20,49]. The IDRs in condensates interact via α-helices hydrophobic attraction [49]. Prior experimental work indicates that isolated blocks of AQ12 can undergo LLPS [45], but the mechanism of the phase separation remains unclear. Notably, since AQ12 contains both hydrophobic amino acids and flexible glycine-rich regions, both entropic and enthalpic factors can promote LLPS. This could lead to both LCST and UCST response, depending on conditions. Indeed, an AQ12-based protein with a highly hydrophobic α-helical terminal domain has been reported experimentally to have a pronounced LLPS transition already at 25 °C [45].

Besides LLPS, large α-helix content can also lead to gelation via secondary structure transition from α-helices to β-sheets. Arndt et al. [52] have demonstrated that another spidroin, NT2-Rep-CT, gels at 37 °C due to secondary structure transitions and aggregation of the NT domains. The gelation of regenerated *Bombyx mori* silk fibroin with temperature increase has also been observed by Nagarkar et al. [53]. Moreover, silk fibroins also gel at low temperatures during storage [54]. In these studies, the gelation by both temperature and time was accompanied by an increase in β-sheet secondary structure [53–55]. Furthermore, peptides with repetitive hydrophobic/hydrophilic motifs tend to form β-sheet-rich gels [56]. Despite the attention that the topic has received, the gelation mechanism of silk-like proteins remains unclear: β-sheet formation but also percolation driven by non-specific interactions further inducing β-sheet formation have been proposed as mechanisms [53,57,58]. Moreover, silk fibroins also gel at low temperatures during storage at low temperatures [59].

Here, we target resolving the molecular processes responsible for gelation of silk-like (AQ12-based) multidomain proteins via elucidating both amino acid and domain specific gelation responses. First, the relation between amino acid sequence and temperature response of the solution interactions in the IDR are extracted by atomistic detail molecular dynamics (MD) simulations. The assembly phase response, its temporal dependencies and the gelation of the corresponding silk-like protein is then mapped experimentally comparing two different types of terminal domains, CBM and FN. Simulating the IDR separately from the terminal domains enables to extract the role of the IDR in the temperature response of the protein. Based on our observations, to aid materials design via post-processing protocol and sample preparation conditions, we propose a simplified assembly phase diagram for the gelation regions separating temperature- and time-induced paths. This, together with the MD simulations that offer molecular-level insight into assembly phase response, paves way for the rational design of silk-protein materials. The findings provide a fundamental framework for the controlled production of silk-like protein hydrogels but also highlight the importance of optimization of their storage conditions.

2. Methods

2.1. Experimental methods

2.1.1. Protein expression and purification

The silk proteins, CBM-AQ12-CBM and FN-AQ12-FN, and isolated terminal domains CBM and FN were cloned into *Escherichia coli* for recombinant protein expression as described previously [47]. Amino acid sequences are presented in supporting information (SI). The expression and purification of the silk proteins were carried out as described by Tunn et al. [47]. No heat treatment step was carried out for CBM, while heat treatment purification was carried out at 60 °C for 30 min for FN. All proteins were further purified using immobilized nickel ion affinity chromatography (Äkta pure, cytiva) by means of HisTrap FF columns (cytiva). After this, the buffer was changed to deionized water using Econo-Pac 10DG gel filtration columns (Bio-Rad Inc.). The purified

proteins were frozen with liquid nitrogen and stored at −80 °C until use.

2.1.2. Sample preparation for gelation tests

The silk-like proteins were concentrated in water with 100 mM NaCl using centrifugal concentrators at 1200 rcf at 20 °C with a 30 kDa cut-off (Vivaspin20, Satorius AG). The isolated terminal domains were concentrated at 2000 rcf at 20 °C (5 kDa cut-off, Vivaspin20, Satorius AG). Unless otherwise stated, the silk-like proteins were concentrated to 1 mM, which is equivalent to 85 mg/ml for CBM-AQ12-CBM and 71 mg/ml for FN-AQ12-FN. To achieve the same mass concentration, the isolated terminal domains were concentrated to 85 mg/ml for CBM and 71 mg/ml for FN. For the heating experiment of CBM-AQ12-CBM (Fig. 4), 1.7 mM protein solution (equivalent to 140 mg/ml) were prepared with centrifugal concentrators at 1200 rcf at 20 °C with a 30 kDa cut-off (Vivaspin20, Satorius AG). This concentration allowed us to observe the sample at LLPS conditions.

2.1.3. Temperature and time stability tests

The temperature stability of the 1.0 mM protein solutions was tested using a thermocycler (PTC-100, MJ Research Inc.) in 0.2 ml tubes filled with 20 μl of the sample. The samples were incubated at 20 °C or heated to 70 °C, respectively 80 °C, for 10 min. To study the effect of temperature on CBM-AQ12-CBM condensate, 20 μl aliquots of a 1.7 mM sample were heated for 10 min at 20, 40, 50, 60, 70, or 80 °C using the same thermocycler described above. All samples were imaged with light microscopy after heating (Zeiss Axio Vert A1, Carl Zeiss AG, 40x/0.6 Ph2 objective lens). The time stability of the silk proteins and the isolated terminal domains was examined by incubation at room temperature until irreversible changes of the samples (gelation, aggregation) were observed. Aging took 12–21 days depending on the sample (see details in the discussion section).

2.1.4. Fourier transformed infrared (FTIR) spectroscopy

The secondary structure of the samples obtained from temperature and time stability test was investigated using FTIR (Spectrum Two, Perkin Elmer). A small amount (10 μl) of the sample was applied to the crystal and spectra were collected with 0.5 cm^{-1} intervals in the range 750–2000 cm^{-1}. The number of averaged accumulations per sample was 16 for all samples, but for the isolated FN protein, the spectra were acquired with 32 accumulations to increase the signal-to-noise ratio. The amide I peak intensity was normalized using OriginPro 2024 (10.1.0.178, academic version).

2.1.5. Circular dichroism (CD) spectroscopy

To study the contribution of the IDRs and the terminal domains to the structural transitions of the silk-like protein with increasing temperature, CD spectroscopy (JASCO J-1500-150ST) was performed. The isolated terminal domains were measured at 0.75 mg/ml protein concentration in 100 mM NaCl, while the silk proteins were measured at 10 μM concentration in 100 mM NaCl in a 1 mm Quartz Suprasil cuvette (Hellma). The spectrometer was equipped with a Peltier element to enable the acquisition of spectra while applying a temperature ramp from 20 to 90 °C with a 1 °C/min heating rate. Spectra were acquired in 1 °C intervals from 200 to 250 nm with 2 s integration time and 1 nm data pitch. The mean residue ellipticity (MRE) [60] was calculated from the data with

$$\theta_{\mathrm{MRE}} = \frac{\mathrm{MRW} \times \theta}{10dc} \tag{1}$$

with the mean residue weight (MRW) (g/mol), the observed ellipticity θ (deg), the path length of the cuvette d (cm), and c the protein concentration (g/l).

2.1.6. Rheology

The rheological properties of the samples were tested using a stress controlled MCR 302 Rheometer (Anton Paar). As a measurement tool CP15-1 (0.03 mm gap) was used and 55 μl of sample was loaded. The sample was sealed with 10 cSt silicone oil to prevent evaporation of water. For the temperature induced gels, the sample was heated to 80 °C with 5 °C/min heating rate to induce gel formation. The temperature was kept at 80 °C for 7 min and lowered to 20 °C and equilibrated for 30 min. For the aged gel the sample was loaded and allowed to equilibrate for 5 min before the amplitude sweep. The amplitude sweep was performed from 0.1 to 1000 % strain at a constant frequency of 10 rad/s to obtain information about the elastic storage modulus G' (Pa) and the viscous loss modulus G'' (Pa), as well as the linear viscoelastic range of the formed gel.

2.2. Molecular dynamics simulations models and methods

2.2.1. Models

For simulating IDRs, the AQ3 sequence was chosen as a model spidroin IDR (see Fig. 1a). This sequence corresponds to three repetitive subunits of the intrinsically disordered part of the AQ12 (eADF3) protein examined experimentally. Simulating the shorter AQ3 sequence enables atomistic detail simulations. While coarse-grained models, such as the recent MARTINI 3 force field for IDPs [61], claim accurate reproduction of IDP conformations, the coarse-graining still leads to incorrect estimation of the entropic contribution to the free energy [62]. This makes temperature response challenging to capture via coarse-grained approaches. The amino acid sequences of the AQ3 and AQ12 proteins are listed in the SI. Three distinct types of silk-like protein systems were examined in water solution: *i*) a single AQ3 chain, *ii*) two AQ3 chains, and *iii*) a fibril model consisting of 36 AQ chains. The first simulation set reveals intraprotein interactions and the effect of temperature on them. The second set *(ii)* enables extracting interprotein interactions and the correlations between inter- and intra-protein interactions, and in *iii*) the fibril mimics conditions expected when the IDR undergoes transition to β-sheet [63].

The length of the AQ3 unit in the simulations of *i*) and *ii*) is 132 amino acids and due to the glycine-rich regions making up 75 % of the protein it is highly flexible. Because of the long, flexible chain, the simulations are run for 1 μs to obtain sufficient sampling to reach reliable intra- and inter-molecular interaction fractions. Opposed to this, in setup *iii*), the crystalline β-sheet-rich region of a fibril was modelled by 36 AQ repeat units set initially into a β-sheet configuration and simulated for 0.5 μs. This was done to compare the stability of β-sheets vs α-helical structures in solvated molecule. Notably, AQ12 can form β-sheets in coacervates [25,61–66]. The shorter AQ sequence is employed because of the crystalline initial configuration. Details of the simulation systems are collected in Table 1 and representative snapshots of the simulated systems are presented in Fig. 1.

For setups *i*) and *ii*), we have assumed that single or two chain simulations allow extracting information on phase transitions in protein solutions. This assumption is common in the field, but not obvious. Indeed, multiple studies have linked the conformation of a single diluted IDP with its phase behavior for a wide range of IDPs [25,64–69]. A clear relation between the critical temperature of the protein solution phase transition and the Boyle temperature (corresponding to vanishing second virial coefficient) has been established [65]. Connecting microscopic and macroscopic measurable quantities are rising from the similar nature of intra- and interprotein interactions of IDPs. The correlation between conformations of single chains and dynamical properties of the condensates [70] have also been established. Furthermore, the relation between single polymer molecule conformation transition in a diluted solution and the corresponding phase transition in a concentrated solution is well-known within homopolymer theory [71,72]. For IDPs, this relation was demonstrated [64] and explained [69] only recently.

Besides this, comprehensive coarse-grained simulations have shown a clear correlation between protein conformation in solution and the

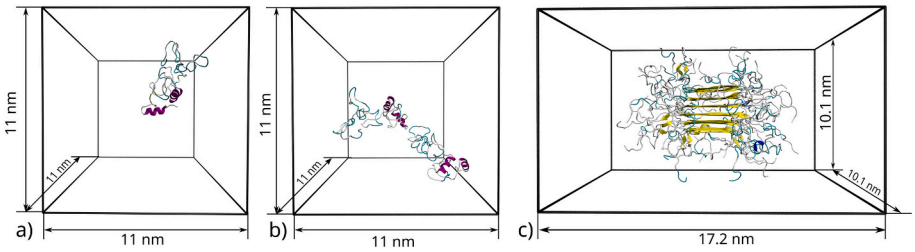

Fig. 1. Snapshots of the simulated systems. a) A single AQ3 protein, b) two AQ3 proteins, and c) model of an AQ fibril, all in their simulation boxes with box dimensions shown. Water as explicit molecules is present in the simulations but omitted in the visualizations. The simulation snapshots visualize representative configurations from the end of the production run of each setup.

Table 1
Summary of the simulated systems, simulation conditions, and system sizes.

System	Number of protein molecules	Total simulation time (ns)	Data analysis time period (ns)	Examined temperatures (°C)	Number of water molecules	Size of the box (nm^3)
Single AQ3 chain	1	1000	800	10, 20, 30, 40, 50, 60, 70, 80, 90	43,448	11.0 × 11.0 × 11.0
Two AQ3 chains	2	2000	1600	20, 60	42,894	11.0 × 11.0 × 11.0
AQ fibril	36	500	450	90	49,684	10.1 × 10.1 × 17.2

phase transitions that its solution experiences over a very wide range of the IDP sequences [70]. Such correlation can be expected to be valid only for long enough chains, and in the studies in which the correlation has been observed it varied from 50 [64] to 167 [65] amino acids. The length of the AQ3 unit in the simulations of *i*) and *ii*), 132 amino acids, falls into this range.

2.2.2. Simulation setup

For the simulations, we used the Gromacs 2022.3 software [73,74]. A common issue in atomistic MD simulations of proteins is the overestimation of protein-protein interactions in contrast to protein-water interactions [75,76]. This can lead to inaccurate prediction of IDP conformations and excessive binding affinity in protein complexes. A possible solution is the reparameterization of the solvent model [77,78]. Here, we use a special force field, Amber03ws, that was developed for simulations of IDPs [79]. The TIP4P-2005s water model, specifically designed for this force field [79,80], is used. Amber03ws has been shown to have a good quantitative agreement with experimental structural data for IDPs [81], particularly for spidroins [49,50,82].

Temperature was controlled by the Nosé–Hoover thermostat [83,84] with a time constant of 1 ps, while pressure was maintained at 1 bar by Parrinello–Rahman isotropic barostat [85] with a time constant of 3 ps. Electrostatic interactions were treated with the particle-mesh Ewald method [86,87] using a cutoff distance of 1.0 nm. The cutoff distance for Lennard–Jones interactions was set to 1.0 nm with the smooth shift to zero at the cutoff distance. The P-LINCS algorithm was used to constrain the bond lengths of the hydrogen atoms [88]. The integration time step was set to 2 fs. For the single AQ3 chains, temperatures between 10 °C and 90 °C, at 10 °C intervals were examined. The total simulation times, the time periods used for data analysis for the different systems, and the corresponding examined temperatures are listed in Table 1.

The equilibration time for each system was determined based on the time evolution of radius of gyration of the protein (R_g) for *i*) (Fig. S1a, b), the number of interprotein contacts in the assembly (Fig. S1c) for *ii*), and the secondary structure of the protein (Fig. S1d) for *iii*). From the total simulations time, the time during which the systems evolved from the initial configuration to equilibrated values of the assessed quantities was omitted in the data analysis. Details of the simulation and analysis protocols are presented in the SI. Data analysis was performed using the Gromacs tools [62,63] and in-house python scripts with use of MDAnalysis library [89,90]. Visualization of the MD trajectories was obtained from VMD [91]. Error estimates correspond to standard deviation of the data. The non-Gaussian distribution box plot shows the first to third quartiles of the distribution. The whiskers in the box plots show data range corresponding to 1.5× the interquartile range from the box in the plot, and the points indicate outliers.

3. Results

3.1. Effect of IDR interactions on LLPS

3.1.1. Solvent quality. Single chain MD simulation

To elucidate the phase response and gelation of AQ12-based proteins, we first examined the solvent (water) quality for the IDR. To achieve this, a single AQ3 chain was simulated. These simulations shine a light into the molecular interactions involved in the temperature dependent response.

Fig. 2a collects the temperature dependent radius of gyration (R_g) of the protein in water. The data shows variation of the AQ3 conformation from a collapsed chain ($R_g = \sim 1.5$ nm, bottom inset of Fig. 2a) to elongated conformations ($R_g = 3.5 - 4.5$ nm, top inset of Fig. 2a) through the entire range of examined temperatures. The R_g distribution does not change significantly as a function of temperature. Therefore, the temperature induced conformational changes were further analyzed by principal component analysis (PCA) carried out on distance matrices of backbone C-alpha atoms, see Figs. S2-S3. The strong correlation observed between R_g and the principal component 1 (Fig. S3) indicates that R_g effectively captures the structural changes that account for the highest variance in the simulations data. This means that the highest structural variability is because of a continuous transition between an elongated and collapsed state in the simulation. PCA has also been previously reported to reveal changes in both the value of R_g [92] and secondary structure [93].

In Fig. 2b, the Flory scaling exponent extracted for the AQ3 chains at different temperatures is presented. It is a measure of the polymer conformation and thus the quality of the solvent [94–96]: a value of $\nu = 0.5$ corresponds to θ-solvent for the polymer, while $\nu < 0.5$ corresponds to a bad and $\nu > 0.5$ to a good solvent. The Flory scaling exponent ν can be extracted by measuring the distance R_{ij} between two separated segments (i and j). Here, these segments were chosen to be amino acids which lead to the following relation

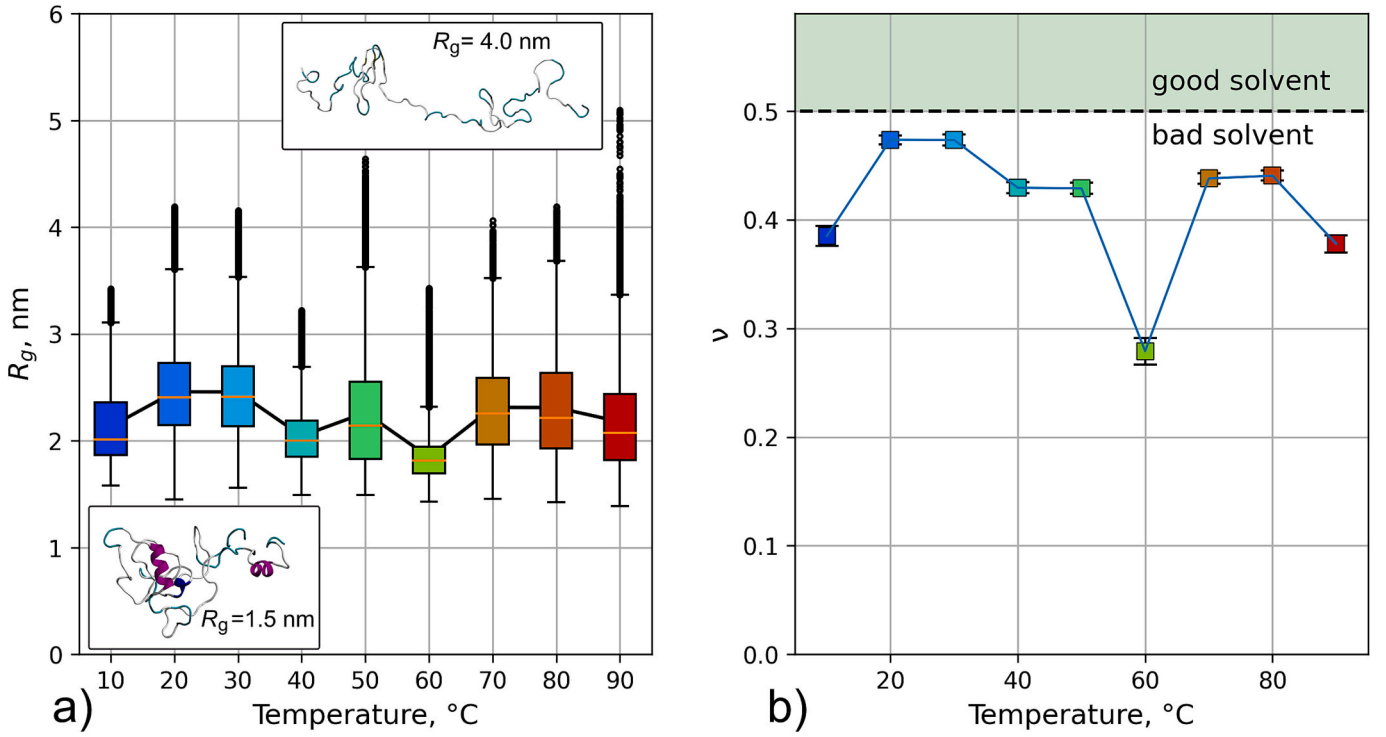

Fig. 2. The temperature dependency of a) the radius of gyration R_g and b) Flory scaling exponent υ of AQ3 protein. The green area in b) shows values corresponding to good solvent conditions, while dashed line at $\upsilon = 0.5$ corresponds to the θ condition of the solution. The colors indicate the temperature of the solution (blue is the lowest temperature, red is the highest temperature). The solid lines provide a guide for the eye showing the change in average values. Insets present illustrations of the protein at $R_g = 1.5$ nm and $R_g = 4.0$ nm, respectively.

$$R_{ij} = b|i-j|^{\upsilon}, \tag{2}$$

where the prefactor b is the effective bond length, equal to Kuhn length for an ideal chain. For IDPs, the average value of b is ~0.55 ± 0.05 nm [65,97]. The ν parameter values for Eq. (2) can be extracted from our simulations data as the linear slope of the logarithmic relationship:

$$\log(R_{ij}) = \log b + \nu \log|i-j|. \tag{3}$$

The detailed results of the fittings to the simulations data are presented in Fig. S4 and Table S1. Notably, the obtained b values range from 0.53 to 0.83 nm (see Table S1), which corresponds to the average b value of IDPs [65,97].

Data of Fig. 2b shows that the value of the Flory exponent υ is lower than 0.5 across the entire examined temperature range. This indicates the low quality of water as a solvent for AQ3. The observation implies that the interactions within the middle IDR of the spidroin can be expected to be a sufficient driving force for phase separation [25,64–66,98,99]. Furthermore, the Flory exponent values indicate a collapsed conformation of the protein in our simulation, which correlates with the IDP conformation in the dilute phase in LLPS systems [100]. This matches with the findings of a recent coarse-grained simulation study where IDPs were more collapsed in the dilute phase than in the dense phase [100]. Also, the results of our simulation explain the observation by Exler et al., who demonstrated the ability of pure AQ12 protein solution to undergo LLPS, but noted the absence of temperature induced phase separation for this protein [61].

However, most ν values are close to 0.5, indicating that the properties of the protein and its phase response can be controlled by small structural modifications, such as changing the folded terminal units, as demonstrated in our recent experiments [62]. The low ν values could be artificial due to poor fitting quality: more collapsed conformations have higher structural correlations within the chain due to specific interactions between amino acids, which affects the fitting quality (Fig. S4). This phenomenon has also been observed for different IDPs [65].

Notably, the simulations were conducted for a shorter protein (AQ3) than the one used in experiments (AQ12). As the molecular mass of an IDP increases, its solubility is expected to decrease [101,102]. The decrease in solubility of AQ12-based protein as a function of molecular weight was also observed in our recent work [72]. Another key factor affecting IDP simulation results is the force field. While many protein force fields are known for protein overbinding and underestimation of protein-solvent interactions [75], the Amber03ws force field used in our study was specifically parameterized to address this issue [79]. Force-field benchmarking studies [79,80] show that Amber03ws has a better balance of interactions. However, in some cases, it underestimates protein-protein interactions [103,104]. This means that the chosen simulation model may overestimate slightly the solvent quality. Nevertheless, this should not affect our simulation results qualitatively.

3.1.2. *Intra/inter-protein interactions from MD simulations*

The IDR conformation in solution is a balance of protein-protein and protein-solvent interactions. For this reason, we next analyzed the temperature dependency of intraprotein and protein-solvent interactions by assessing the hydrogen bonding and aggregation of the Ala regions that form hydrophobic α-helices at different temperatures. The data is presented in Fig. 3, where panel a) presents hydrogen bonding, both within the protein and between the protein and the water molecules, and panel b) the number of contacts between Ala regions.

Fig. 3a shows that hydrogen bonding between the protein and the solvent decreases with increasing temperature. A two-stage drop in the number of hydrogen bonds is observed: first between 10 °C and 30 °C, and then between 60 °C and 70 °C. Likewise, intraprotein hydrogen bonding also decreases. This response is opposite to the LCST response of elastin-like peptides [66,105–107]. However, Fig. 3b shows that the hydrophobic interactions, measured here as contacts within the Ala-rich regions, increase with temperature. Furthermore, at temperatures of

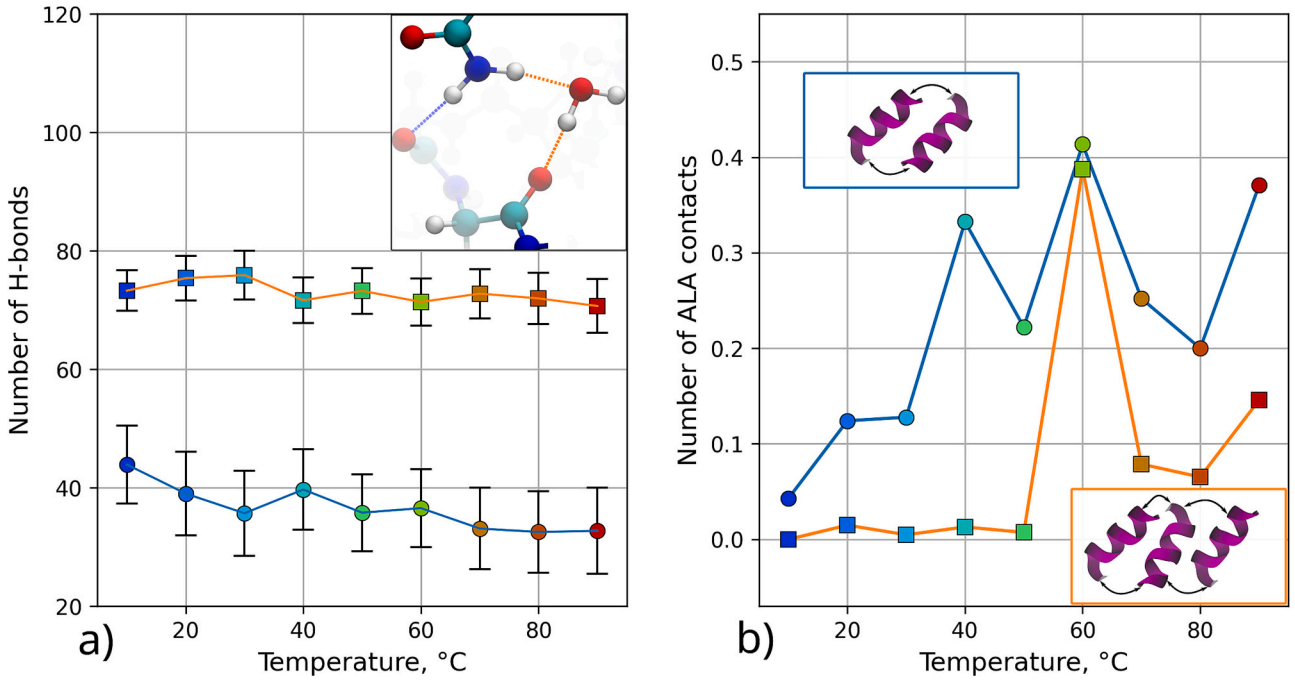

Fig. 3. Temperature dependence of a) the average number of protein hydrogen bonds (orange line with square markers - with solvent, blue line with circle markers - intraprotein). Inset presents a visualization of hydrogen bond between protein and water (orange dashed lines) and intraprotein hydrogen bond (blue dashed line). b) The average number of hydrophobic contacts between Ala-rich domains over the simulation time (blue line with circle markers - single contact, orange line with square markers - multiple contacts due to Ala clustering). Insets illustrate the scheme of single and multiple hydrophobic contacts between the helix forming Ala-rich domains.

60 °C and above, the Ala-rich domains show a clear tendency to aggregate. This quite expectedly keeps the protein molecule in a collapsed conformation. The negative correlation between the R_g values and the number of contacts between the hydrophobic Ala-rich domains increases with the temperature (Fig. S5). In the multiprotein system, interprotein interactions replace some intraprotein interactions, but the temperature response observed for the single AQ3 persists (Fig. S6). As noted, the protein remained mainly in collapsed conformations (Fig. 2). The change of the interaction balance reveals that the overall hydrogen bonding is decreasing while hydrophobic contacts are increasing with the increase of temperature. At different temperature ranges, the collapsed configuration is a result of different protein interactions. At high temperatures, hydrophobic interactions prevail, and at low temperatures hydrogen bonding is dominant. Contact map information is provided as Fig. S6.

Notably, recent studies have highlighted the significant role of tyrosine (Tyr) amino acids in the phase transition of various silk-like proteins and materials based on them [44,108–110]. However, in our simulations, we did not observe π-π stacking involving Tyr amino acids, and their hydrogen bonding was similar to the one of glutamine (Gln) amino acids (see Fig. S7).

It is important to note that the AQ12 sequence lacks charged amino acids, leading to the absence of cation-π interactions. This contrasts with other silk proteins, such as the NT-2Rep-CT protein, where the IDR contains both Tyr and arginine (Arg) amino acids. In this case, cation-π interactions explain the importance of Tyr for NT-2Rep-CT phase separation observed previously in multiple studies [108,110]. Recently, Landreh et al. [109] proposed the "sticker-spacer" model of spidroins, where Tyr acts as a "sticker" and other amino acids, including Ala, serve as "spacers." Based on our simulation results, we propose that for the AQ12-based proteins, it would be more accurate to consider the Ala-rich domains as "stickers" and the glycine-rich domains (including Tyr) as "spacers." In this context, it is important to highlight a recent publication by Hu et al. [111], which demonstrated the crucial role of the Ala sequence in the assembly response of spidroins. The length of the Ala motifs in the protein significantly affects the assembly response: short motifs lead to silk nanofibrils that are prone to disassembly, while long motifs result in nanofibril aggregates that resist disassembly upon dilution [111].

3.1.3. *Phase separation and gelation of CBM-AQ12-CBM*

The balance of protein-protein interactions revealed by the data in Fig. 3 results in complex temperature-dependent phase response of AQ3-based proteins. Phase separation is governed by hydrophobic interactions at high temperatures, while at low temperatures it is due to the increase in conformational entropy [109]. Considering the simulation results on AQ3, the longer CBM-AQ12-CBM sequence can also be expected to exhibit phase separation. We pursued experimental verification of this, obtaining an indirect confirmation from a solution of CBM-AQ12-CBM protein at 1.7 mM protein concentration (Fig. 4).

In Fig. 4, the microscopy images show that from 20 °C to 60 °C the solution contains protein condensates. Most of the observed condensates were liquid-like (spherical condensates that exhibit fusion and growth) but some were solid-like aggregates (irregular shaped condensates that do not fuse). This is consistent with the assumptions made based on our MD simulations, and it indicates that water acts as a poor solvent throughout the examined temperature range. Specifically, phase separation into protein condensates is observed at the examined temperatures. In the experimental characterization, the examined protein construct includes, in addition to the IDR, also the CBM terminal domains. The terminal domains can influence the system phase response. Specifically, the interactions between CBM terminal domains [82] can be expected to increase the temperature range corresponding to the phase separation region due to the hydrophobic motifs on its surface [112]. At 70 °C, the sample gelled. Similar temperature-induced gelation has been observed for different silk proteins, and it has been associated with the formation of β-sheet structures [52–55]. However, resolving the molecular mechanisms of gelation requires additional research. Reflecting this, Nagarkar et al. [53] proposed that protein aggregation and fibroin gelation can be caused by β-sheet formation

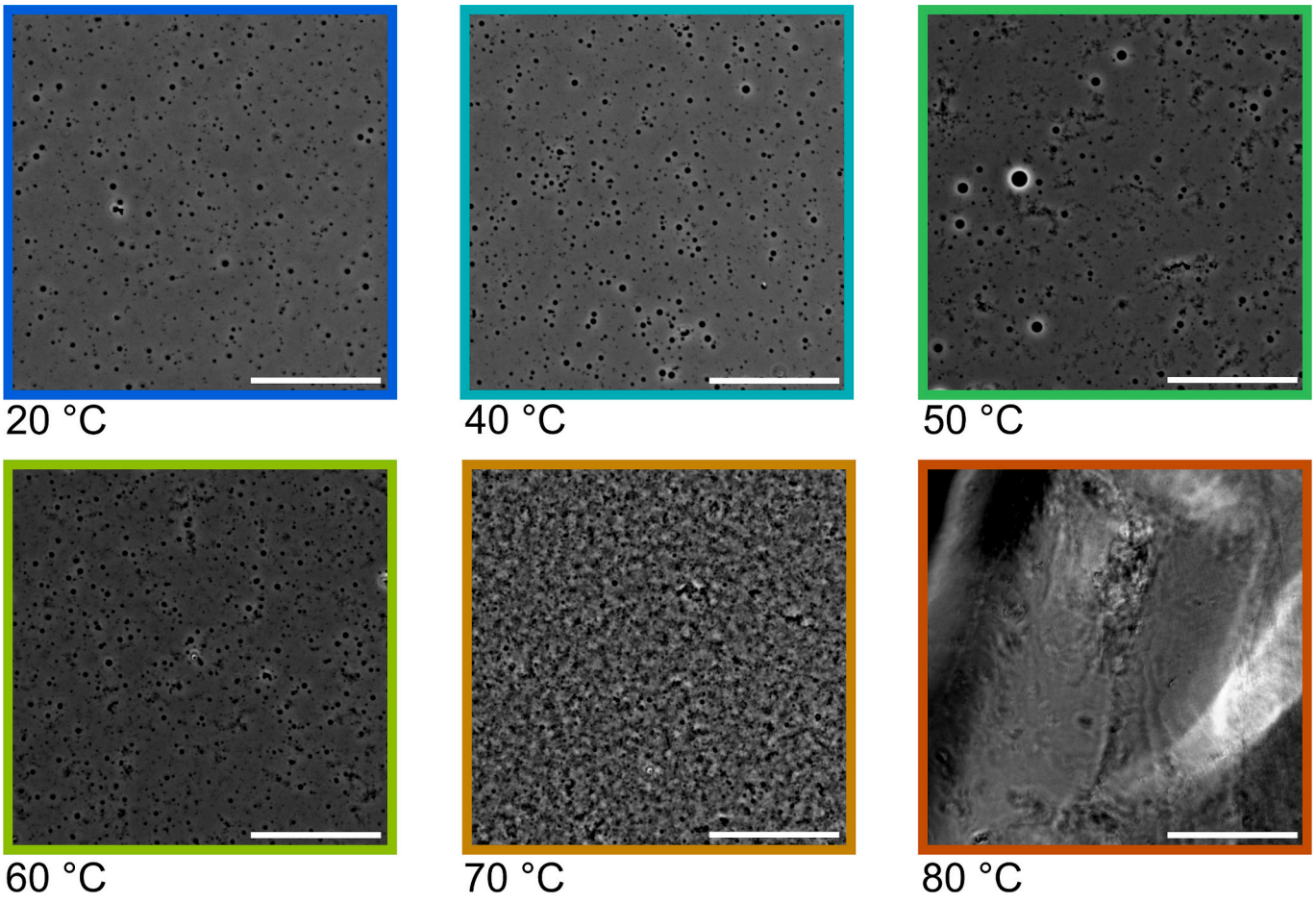

Fig. 4. Microscopy images of CBM-AQ12-CBM 1.7 mM solution at different temperatures. In the temperature range 20 to 60 °C, the solution contains protein condensates. At 70 °C and above, the sample is homogeneously gelled. The scale bar is 50 μm.

inducing association. Matsumoto et al. [109] observed that early stages of gelation can take place without β-sheet formation. However, as gelation can also be governed by specific interprotein interactions [110], changes in the amino acid sequence can significantly bias the molecular mechanisms of gelation. Inspired by this, we studied secondary structure changes as a function of temperature and its effect on gelation.

3.2. Temperature-induced gelation

3.2.1. CD and FTIR analysis

To reveal the molecular mechanism of gelation, we next analyzed the secondary structure of the proteins, both experimentally and with simulations, at different temperatures. The experimental protein concentration was chosen in such a way that coacervation was minimal for simplicity of the setup. The protein concentration was set to 1.0 mM to achieve this. In agreement with prior findings on fibroin proteins [111], here we found that gelling of the recombinant AQ12-based proteins is accompanied by β-sheet formation. The corresponding FTIR and CD data for CBM-AQ12-CBM is presented in Fig. 5. For FN-AQ12-FN, the data is presented in Fig. S8.

The stretching mode of C═O groups in the peptide backbone (amide I) serves as an indicator of protein secondary structure: β-sheets contribute to the signal at 1610–1640 cm^{-1}, while α-helices and disordered structures are associated with signals at 1650–1660 cm^{-1} and 1640–1650 cm^{-1}, respectively [113]. Thus, the rapid shift of the amide I band maxima from 1635 cm^{-1} (at 20–70 °C) to 1621 cm^{-1} at 80 °C indicates a rise of β-sheet content. A similar response on the FTIR signal was observed during the crystallization of silk fibroin by Hu et al. [114]. The same transition to more ordered structures around the gelling temperature was observed at low protein concentrations (10 μM) by CD (Fig. 5a, b). The minima of the CD spectrum at 216 nm and at 20 °C indicates a high content of β-sheets [115]. This results from the folded β-sheet structure of the CBM. A temperature increase from 20 °C to 70 °C leads to only a slight monotonic decrease of CD signal at 216 nm, which indicates an increase in ordered structures. Closer to gelling temperature, at approximately 80 °C, a rapid increase of β-sheet secondary structure was observed in the CD spectra. The observed increase in ordered structures is consistent with a recently reported study of temperature induced secondary structure of silk-based coating [114].

As both CD and FTIR show similar secondary structure changes with temperature variations across different concentrations and assembly phases where the measurements were carried out, the secondary structure changes are independent of gel formation. In contrast to CBM-AQ12-CBM, the FN-AQ12-FN protein experiences an increase in ordered β-sheet structures with increasing temperature over the whole temperature range tested (shown by both methods, CD and FTIR), with gelation occurring at 70 °C (see Fig. S8). This phenomenon is attributed to the secondary structure transitions of FN terminal domains, as evidenced by the behavior of isolated FN protein (see Fig. S9).

To determine the role of the middle IDRs in temperature-induced gelling, we performed the same experiments using terminal domains only (CBM and FN) (see Figs. S9-S10 in the SI). Notably, an increase in temperature did not lead to gelation in the solutions. However, the terminal domains formed finite-sized aggregates. Furthermore, based on the FTIR and CD data detected, CBM does not change secondary

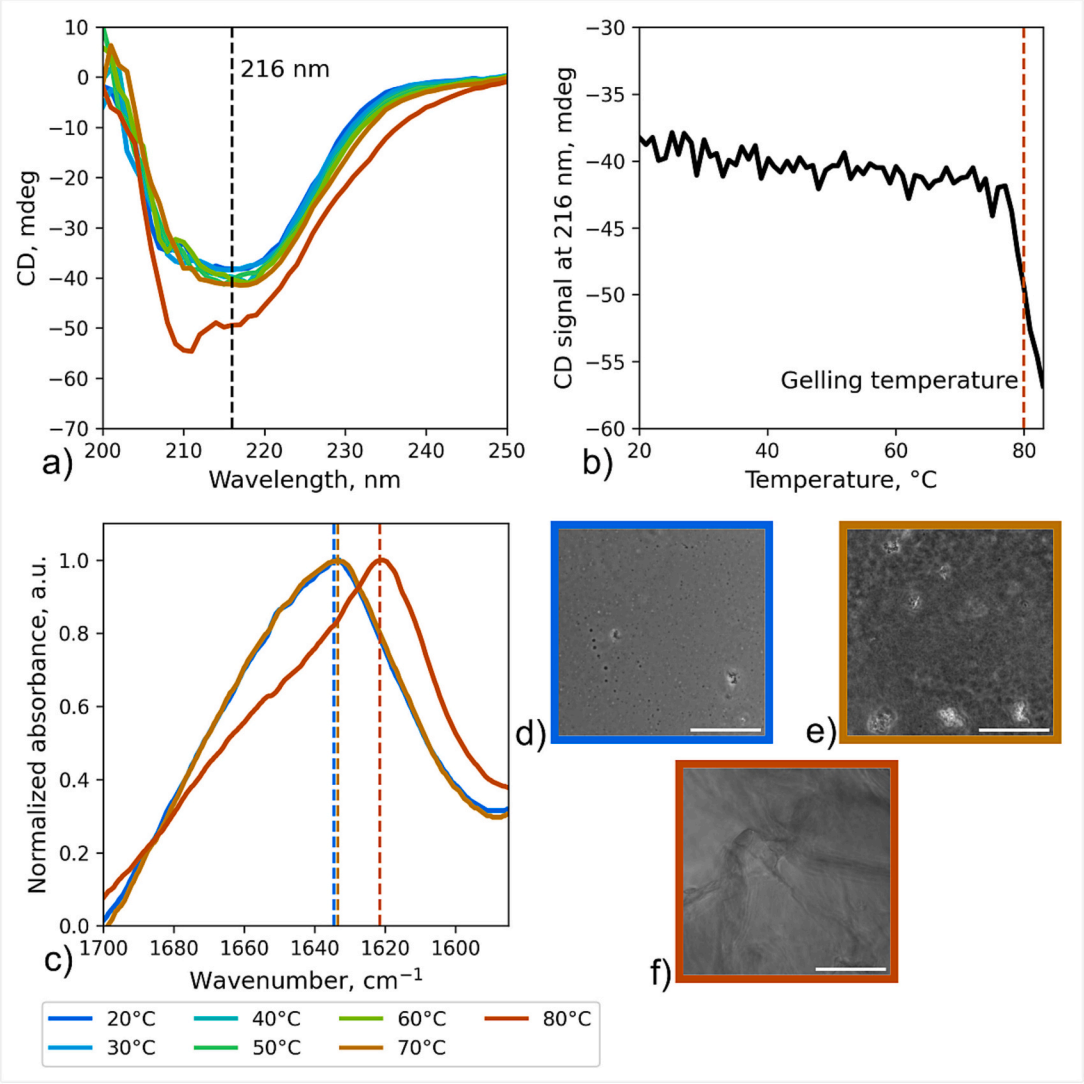

Fig. 5. The effect of temperature on CBM-AQ12-CBM secondary structure. a) CD data from 20 to 90 °C (protein concentration is 10 μM). b) The change of CD signal at 216 nm with temperature, indicating an increase of ordered structures. c) FTIR data of CBM-AQ12-CBM solution (protein concentration is 1.0 mM) for temperatures 20 °C, 70 °C, and 80 °C, respectively. The vertical dashed line on FTIR data (panel c) indicates a shift of the maxima of the amide I band as a function of temperature. d-f) Optical microscopy images illustrating the state of the sample at 20 °C, an increase of turbidity at 70 °C, and gelling at 80 °C (protein concentration is 1.0 mM). The scale bar is 50 μm.

structure in the studied temperature range (see Fig. S10). This indicates that the observed structural changes mainly occur in the silk-like proteins IDRs.

Unlike CBM, FN experienced a conformational change with temperature (shown both by CD and FTIR) (see Fig. S9). FN showed a shift of the amide I band in FTIR spectra in the range 1635 cm^{-1} to 1622 cm^{-1}, indicating an increase of the β-sheet structures. A similar temperature response has been reported for the entire fibronectin construct by Pauthe et al. [116]. They observed an increase in the signal corresponding to β-sheets accompanied by protein aggregation and proposed that the formation of intermolecular β-structures occurs through partial unfolding of the initial structure and transformation of turns to additional β-sheets. Interestingly, the fibronectin thermostability study by Litvinovich and Kenneth [117] suggested that the less thermostable domain, module 9, is responsible for these changes. However, we observe a similar shift in the FTIR spectra of the here studied module 10. This indicates the appearance of additional intermolecular β-sheet structures at higher temperatures (80 °C), which remains below the reported melting temperature of this domain (>110 °C [117]). The temperature of 80 °C is, however, probably sufficiently high to enable partial unfolding and further aggregation. The formation of the β-sheet aggregates can be expected to result in additional crosslinks, and to affect the properties of FN-based hydrogels.

3.2.2. *Molecular mechanisms of gelation*

To reveal the molecular mechanism of the observed gelation response of the IDR, we analyzed the effect of temperature on the IDR secondary structure using atomistic detail molecular modelling of the solvated AQ3 protein and the same AQ sequence with only one AQ unit (AQ1) as a fibril. Fig. 6 illustrates the change of the secondary structure in a single solvated AQ3 chain with increasing temperature. The analysis details are provided in the SI. The data show how the ordered and disordered structure changes with increasing temperature, and the distribution of lifetimes of the conformations of Ala related to ordered structures for a model of single solvated chain (α-helices) and the model of a fibril (β-sheets). Detailed secondary structure analysis data are presented in Fig. S11.

Single-chain simulations show a significant decrease in the helical content and an increase in disordered structures with increasing temperature. The largest contribution to the helical content comes from

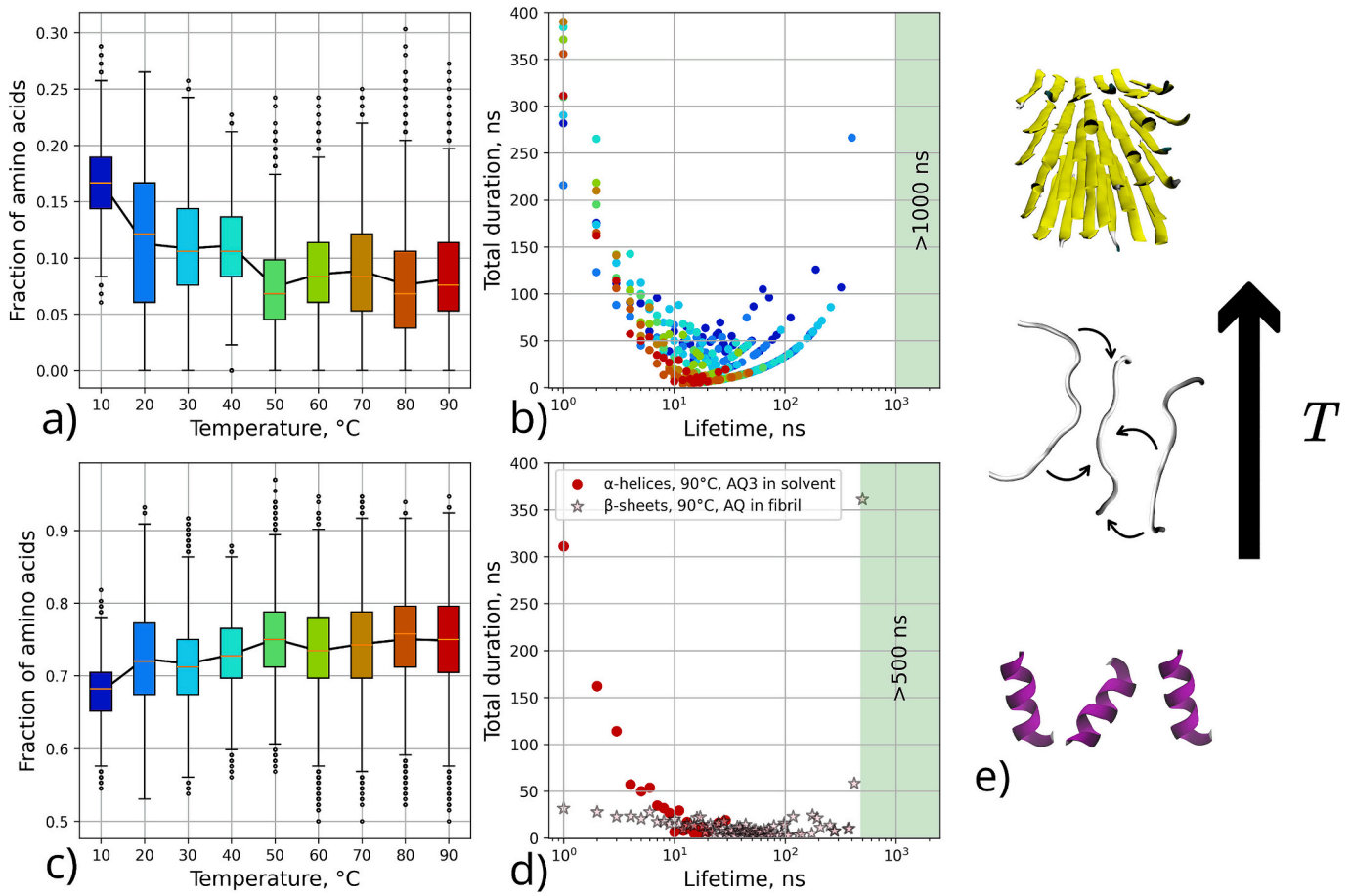

Fig. 6. Temperature dependence of the protein model secondary structure and lifetimes of the conformations corresponding to ordered secondary structures (helices for single protein and β-sheets for the fibril model). a) Fraction of amino acids in helices in AQ3 single protein. b) Total α-helix lifetime duration in AQ3 protein solvated in water solution at different temperatures. c) Fraction of amino acids in disordered structures in AQ3 single protein. d) Total lifetime durations of ordered structures in a single AQ unit of AQ3 protein (α-helices) and in an AQ1 fibril (β-sheets). Lifetimes were calculated as the duration that individual amino acids remained in a conformation associated with a specific secondary structure. The total duration of a specific lifetime weights the data to show the impact of a specific secondary structure in the conformations. It is calculated as the sum of the observed individual events corresponding to that particular lifetime. The details of the analysis are provided in the SI. Most β-sheet structures in the fibril simulation remain stable the entire simulation time (500 ns), signifying that their lifetimes exceed 500 ns. The coloring indicates temperature (with blue corresponding to low temperatures and red to high temperatures). e) A schematic cartoon visualizing the molecular mechanism of the formation of β-sheet crystals with temperature increase.

α-helices (Fig. S11). At 10 °C, the fraction of helices is 0.17. This implies that almost all Ala-rich regions (a fraction of 0.18 of the AQ3 protein) are in α-helical conformation. When the temperature increases further, the average fraction of helices decreases to 0.08 at 50 °C (Fig. 6a). This means that as α-helices form the ordered structure in the AQ3 protein, half of the amino acids that are in ordered structures at lower temperatures become disordered at 50 °C. Furthermore, the remaining helices are highly unstable at higher temperatures (Fig. 6c). At 90 °C, the maximum lifetime of the Ala helical conformation was below 50 ns, which is an order of magnitude shorter lifetime than at 10 °C. In contrast, in the fibril, Ala conformations in β-sheet crystals remained stable for temperatures up to 90 °C for the entire 0.5 μs simulation. Actually, almost all Ala amino acids in the fibrils maintained their secondary structure conformation for the entire simulation time [118]. These results are consistent with previous experimental observations of the stability of poly-Ala ordered structures [119,120], which also demonstrate the higher thermal stability of β-sheets compared to α-helices.

The discussed observation explains the drastic increase in β-sheet content with increasing temperature (see CD/FTIR data in Fig. 5). The temperature-induced conformational change accompanied with aggregation of hydrophobic Ala-rich regions is the main driving force of gelation. As a result, the β-sheet crystals act as crosslink connection nodes in the silk-protein hydrogel structure and determine its main properties, such as mechanical [121] and thermal [122,123] characteristics, as well as biodegradation rate [124,125]. Furthermore, the structural rearrangements between different ordered and disordered structures could affect interface interactions in silk-based composite materials. This affects especially preparation protocols involving temperature treatment during preparation, see for example Refs. [21, 126].

3.2.3. *Time-induced gelation*

In a molecular system where a transition between two states is governed by one primary process that associates with an energy barrier, the process rate can be expected to be governed by Arrhenius's law, which represents the exponential relation between temperature and reaction rate. For the silk-protein system, such a process could be, e.g., gelation. However, protein gelation is known to occur through different mechanisms for both globular proteins and IDRs. Gelation can occur for example through dynamic arrest of globular proteins due to their high concentration and attractive interactions [52,125], the denaturation of a globular protein and its further aggregation [52,127], or the percolation of IDRs, as well as suppression of their dynamics through specific interprotein interactions [128]. Here, the increase in temperature drives gelation of AQ12-based proteins via the interaction between Ala-rich regions, which is due to strengthening hydrophobic interactions and

secondary structure transitions.

Temperature and time-induced structural transitions in silk-like protein solutions are likely to result from different interactions, such as from changes in hydrophobic (entropy driven) interactions at low and high temperatures. At low temperatures, non-hydrophobic interactions may be governing, while at high temperatures hydrophobic interactions may become more prominent. This could lead to different gelation mechanisms. Fig. 7 presents the comparison of the structures resulting from temperature-induced and time-induced structural changes of the silk proteins studied by FTIR spectra, and optical microscopy images of the silk proteins along with a comparison with their temperature-induced gels. The studied systems correspond to the silk-protein solution aged for 12–14 days, with the time determined based on the day of the observed protein aggregation and further sedimentation or/and homogenous gelation.

The microscopy images of Fig. 7 show that the time-induced changes differ from those induced by temperature. Both studied proteins, FN-AQ12-FN and CBM-AQ12-CBM, exhibit similar responses to temperature, both in terms of gelation and secondary structure changes, as discussed in detail above. However, aging at room temperature leads FN-AQ12-FN to gel uniformly throughout the solution volume, while CBM-AQ12-CBM aggregates and sediments. For both proteins, minimal changes in secondary structure over time take place. This can be seen by the shift of the amide I band being insignificant with the maxima shifting from 1636 cm^{-1} to 1634 cm^{-1} for FN-AQ12-FN and from 1635 cm^{-1} to 1634 cm^{-1} for CBM-AQ12-CBM (Fig. 7a, b). This demonstrates the ability of AQ12-based proteins to gel without forming β-sheets. Here, the gel formation is driven by the combination of the interaction of both IDR and terminal domains. However, given that the β-sheet structure is energetically more favorable [120], structural rearrangements are expected to occur with further aging.

To investigate the differences between the temperature-induced and aged gels, we conducted rheological characterization. The amplitude sweeps reveal that the elastic storage modulus G' of the aged gel is about 3 times higher compared to the temperature-induced gel. The higher G' of the aged gel might be due to a higher amount of network connections via entanglements of the silk protein, that can form with time. In addition, the shape of the amplitude sweeps, i.e. the linear-viscoelastic (LVE)-range, is different for the two types of gels. The LVE-range provides information about the onset of irreversible changes to the gel network when applying stain. While the temperature-induced gel is LVE up to about 300 % of strain, the time-induced gel has a LVE range of only 10 % strain. This indicates that different types of crosslinks are present in the aged vs. temperature-induced gels. According to the FTIR data, these differences might originate from the presence of β-sheets formed by the poly-Ala stretches in the AQ12 midblock in the temperature-induced gels while no additional β-sheets form in the aged gel.

The FTIR and optical microscopy results correlate with a prior study

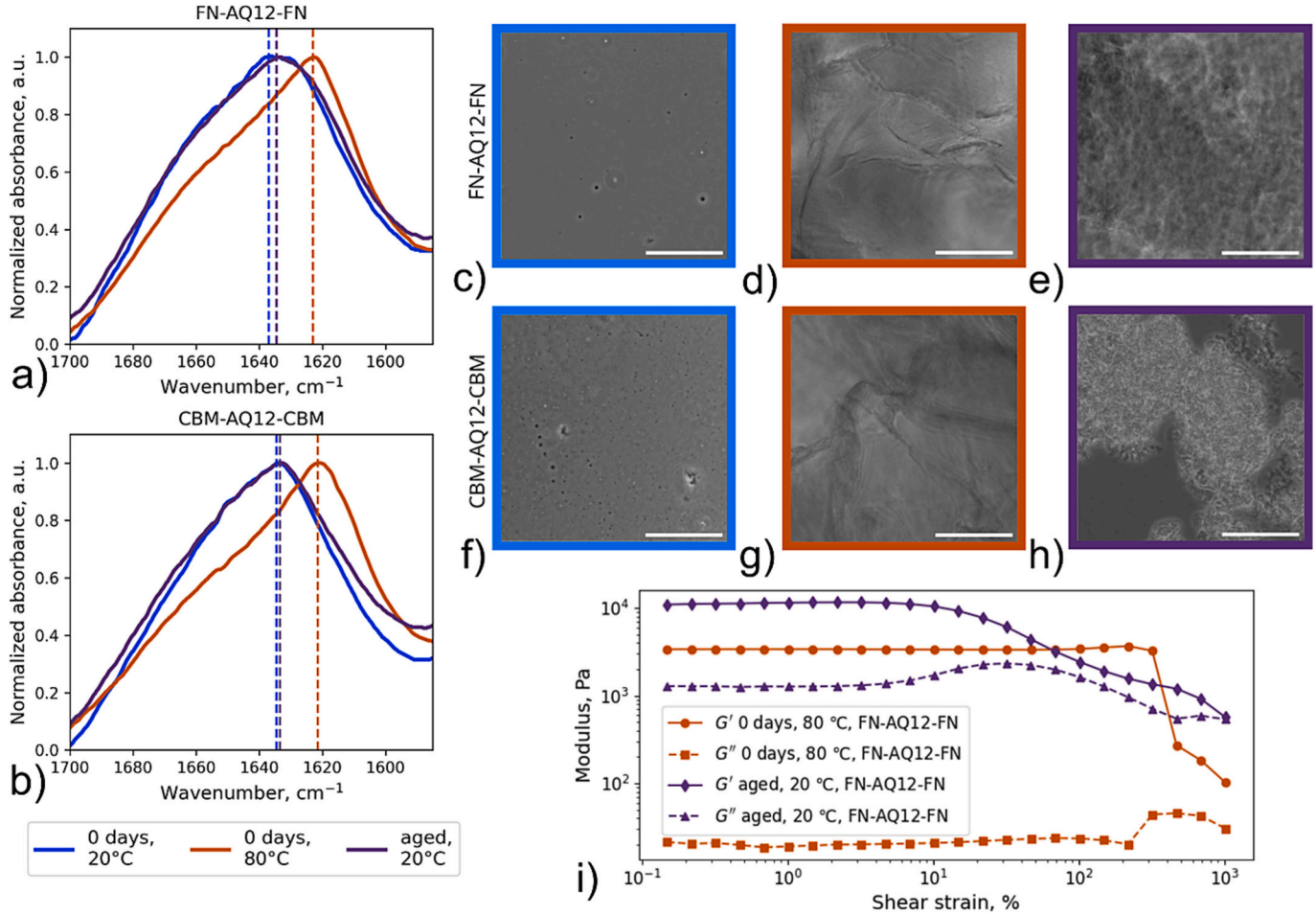

Fig. 7. Comparison of initial, temperature-treated (80 °C), and aged silk protein systems. a, b) FTIR data of FN-AQ12-FN and CBM-AQ12-CBM solutions, respectively. The vertical dashed line on FTIR data indicates a shift of maxima of the amide I band. c-e) Microscopy images of FN-AQ12-FN solution corresponding to FTIR data (initial, temperature-treated (80 °C), and aged systems). f-h) Microscopy images of CBM-AQ12-CBM solution corresponding to FTIR data (initial, temperature-treated (80 °C), and aged systems). For aged samples, data was collected when irreversible visual changes were observed. For CBM-AQ12-CBM aging is 14 days, while for FN-AQ12-FN it is 12 days. i) Rheological characterization of the time-induced and aged gels of FN-AQ12-FN with a strain amplitude sweep. Protein concentration is 1.0 mM and scale bar 50 μm.

of silk fibroin proteins, which revealed that at room temperature the fibroin undergoes a preliminary step of gelation without an increase in β-sheets. Notably, solutions of isolated terminal domains without IDRs are more stable and require a longer aging time to observe the irreversible protein aggregation (Fig. S12). These observations are in line with our conclusions from the simulations that AQ12 has poor solubility in water.

The aggregation and gelation of tri-block silk-like proteins at low temperatures observed over time is governed not only by hydrophobic interactions between the Ala-rich domains of the IDR, but also by the terminal domains. Difference in aging processes between CBM-AQ12-CBM and FN-AQ12-FN can be explained by the difference in the percolation threshold of these two protein constructs which is the critical concentration at which the protein forms a spanning network [36,128,129]. At the studied conditions, CBM-AQ12-CBM has a higher percolation threshold than FN-AQ12-FN. The higher percolation threshold of CBM-AQ12-CBM results in the formation of protein aggregates which sediment without forming the system-spanning network required for gelation at 1.0 mM protein concentration. Notably, in a prior study, we have demonstrated the significant effect of the terminal units on the properties of the protein solution and LLPS [127–129]. CBM and FN exhibit substantial differences in interaction strength, directional anisotropy of binding, as well as the nature of their interactions [128–130]. All these factors drastically affect the percolation threshold [130–132], which makes it challenging to identify a single reason for the difference in aging.

3.2.4. *Proposed minimalist "phase" diagram*

Recently, we showed similar temperature and time response for solutions of a minispidroin NT-2Rep-CT [128]. NT-2Rep-CT has a tri-block structure analogous to the proteins investigated in the current study [129]. We used a minimalist "phase" diagram to demonstrate that the NT-2Rep-CT solution has an intricate temperature vs time response in its assembly, including metastable LLPS, dynamically arrested aggregates, and also gel states [130]. Solution metastability and the stochastic nature of the dynamic arrest led to a temporal evolution (aging) of the protein solutions [131]. In the current work, we observed a similar response for AQ12-based silk proteins. This response is summarized in Fig. 8, which presents the simplified "phase" diagram based on our observations of the protein system studied here. It is important to note that by definition, a phase diagram only represents equilibrium phases [133]. The presented and discussed "phase" diagram shows also metastable and dynamically arrested states and consequently does not adhere to the formal definition of a phase diagram. While state diagram would be a more appropriate term, the widespread use of phase diagrams in the literature prompts us to use the term "phase" diagram also here [109,134].

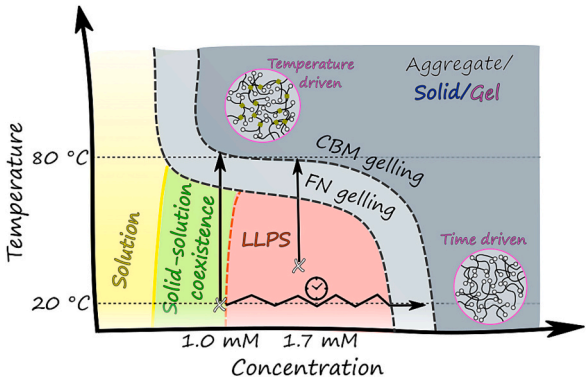

Fig. 8. A simplified "phase" diagram summarizing the protein solutions phase and assembly response at initial time (upon sample preparation) and showing the temporal evolution (aging) of the solution. Phase boundaries are shown in color and a high probability of dynamic arrest in black dashed lines. Solid-like and dynamically arrested states observed in the experiments are represented by the gray region. The gelation mechanisms identified for the AQ12-based proteins in our work are presented by two different pathways. First, the solid vertical arrows show the temperature-induced change to gel. Second, the temporal evolution is represented by horizontal squiggly arrows of the samples at fixed temperatures to the dynamically arrested states. The light gray area identifies a difference in the propensity of dynamic arrest of tri-block protein with the two different terminal units studied here (CBM and FN). The two inset circles visualize temperature-driven and time-driven mechanisms responsible for gelation.

We observed LLPS and the formation of finite sized aggregates or system spanning gels for the investigated temperature range (20–80 °C) and both examined concentrations (1 and 1.7 mM) of the two studied AQ12-based protein solutions, see Fig. 8. Similar to our recent work on NT-2Rep-CT solutions [24], the finite sized aggregates and system-spanning gels observed in this work for the AQ12-based proteins are likely to result from dynamic arrest. The type of terminal domains influences strongly the AQ12-based proteins assembly response, especially temporal evolution (aging). For example, at 1 mM and 20 °C FN-AQ12-FN forms system-spanning gels while CBM-AQ12-CBM forms finite-sized aggregates. Interestingly, at the same mass concentration, solutions of isolated terminal units show higher resistance to gelation (Fig. S11). The IDRs in the protein enhance entanglement, akin to polymer solutions, and this is known to increase propensity for dynamic arrest [135]. Additionally, attractive sites, such as the Ala-rich regions, can be responsible for a slowing down of the dynamics [51,136]. For the AQ12 system at room temperature, entanglement is likely to be one of the main drivers for dynamic arrest (bottom inset in Fig. 8).

On the other hand, at higher temperature, all studied samples formed system-spanning gels with the formation of β-sheets between Ala-rich regions, which act as crosslinks in the network (top inset of Fig. 8). The gelling temperature (70–80 °C) was much higher than in the case of the previously investigated NT-2Rep-CT protein (37 °C) [24], which is due to the difference in the amino acid sequence of proteins. In the case of AQ12-based proteins, the gelling is governed by Ala-rich regions, whereas for NT-2Rep-CT, it is driven by the aggregation of terminal units [52].

A similar difference was observed in the aging time necessary for irreversible gelation to occur. For NT-2Rep-CT, irreversible aggregates formed after two days [24]; however, for AQ12-based protein (at four times higher concentration), it took 12 days. Although the temperature and time required for gelling significantly vary between the work of Ref. [24] and our data studying different protein constructs, the results clearly point toward dynamic arrest being important in forming silk-like protein materials. This underlines the crucial role of the processing pathway in making silk-based materials [24].

4. Conclusions

In this work, we focused on the temperature and time dependent assembly responses of tri-block silk-like proteins with AQ12 as the middle IDR segment and CBM or FN as terminal units. Molecular level mechanism differences for the temperature and time driven changes were charted by combination of MD simulations and experimental characterization of the assembly dependencies by light microscopy, CD and FTIR spectroscopy. At molecular level, the MD simulations revealed that the AQ3 fragment of the longer AQ12 is poorly soluble in water over a broad temperature range, evidenced also by our experimental characterization of the respective proteins over a wide temperature range between 10 and 90 °C. For the triblock protein (CBM-AQ12-CBM), this meant that the intrinsically disordered middle part, the AQ12 sequence, decreased the solubility of the protein. This led to the triblock protein being able to undergo liquid-liquid phase transitions over a wide temperature range.

The broad temperature range for the liquid-liquid phase separation of the AQ12-based silk-like proteins rises from the altering hydrophobic

Ala-rich domains and hydrophilic disordered glycine domains. Temperature increase led to protein-protein interactions changing. Increasing temperature decreased the number of hydrogen bonds between amino acids, but glycine-rich domains contributed to increasing the free energy contribution via conformational entropy in the MD simulations. Increasing temperature also made the hydrophobic interactions within the Ala-rich region stronger, leading to the insolubility of AQ12 at high temperatures.

Light microscopy demonstrated that the AQ12-based protein solutions form system spanning gels at high temperatures (>80 °C). Consistently, CD, FTIR and MD simulations pointed to the molecular mechanism of this transition being based on secondary structure changes. At low temperatures, the Ala-rich regions formed stable α-helices but at high temperatures they clustered, which, together with the decreasing stability of α-helices, led to β-sheets as the energetically more favorable structure. The β-sheets acted as crosslinks in the temperature-induced gels.

The AQ12-based triblock protein solutions at room temperature experienced dynamic arrest during the aging of the samples. The solutions response in time showed that the interaction between the terminal domains is more important at lower temperatures than the weaker hydrophobic interactions between the IDR domains in determining the protein solutions response. This can be interpreted as different terminal domains leading to different assembly states when aging. This is demonstrated by the CBM-AQ12-CBM protein solution forming aggregates and sedimenting while the FN-AQ12-FN protein solution forms system-spanning gels. In both cases, the secondary structure did not change with aging. This is a clear difference from the high-temperature gelation, where the mechanism is β-sheet formation of Ala-rich regions. At room temperature, percolating proteins entangle, and this combined with the interactions between the terminal domains and the IDR domains cause gelation. The differing gelation mechanisms in terms of underlaying interactions resulted in different percolation thresholds for the different terminal units. Consequently, this led to the CBM-AQ12-CBM and FN-AQ12-FN protein solutions behaving differently in their assembly response and their time evolution.

Additionally, we used a simplified "phase" diagram to summarize our computational and experimental observations. The "phase" diagram approach aids in generalizing the results and developing approaches for designing protein-based materials. Priorly, we have observed similar "phase" behavior also in another spidroin, NT-2Rep-CT protein, but with significant differences in gelling temperature and aging time [24]. The differences in the findings here highlight the importance of the protein's amino acid sequence in the assembly response.

We identified and reported two different mechanisms of gelation (temperature and time-induced) for the same system, which enable fine-tuning of the resulting gel properties. The significance of differentiating the gelling mechanisms is that this enables designing solution preparation parameter combinations in which optimal protein percolation and β-sheet formation are coupled to the control of temperature and time of incubation of the protein solution. The molecular level dependencies revealed in this work highlight the potential for engineering gels from silk-like proteins by adjusting protein composition and temperature. The findings also draw attention to the importance of the preparation protocol. Specifically, we identified time as a separate variable dimension to the physicochemical molecular characteristics and sample conditions in understanding and engineering the self-assembling protein materials and their gelation response.

CRediT authorship contribution statement

Dmitry Tolmachev: Writing – review & editing, Writing – original draft, Visualization, Software, Methodology, Investigation, Formal analysis, Data curation, Conceptualization. **Isabell Tunn:** Writing – review & editing, Visualization, Methodology, Investigation, Formal analysis, Data curation, Conceptualization. **Adam L. Harmat:** Writing – review & editing, Visualization, Formal analysis, Conceptualization. **Nea B. Möttönen:** Investigation, Data curation. **Alberto Scacchi:** Writing – review & editing, Funding acquisition, Conceptualization. **Markus B. Linder:** Writing – review & editing, Supervision, Resources, Project administration, Conceptualization. **Maria Sammalkorpi:** Writing – review & editing, Supervision, Resources, Project administration, Funding acquisition, Conceptualization.

Declaration of competing interest

The authors declare that they have no known competing financial interests or personal relationships that could have appeared to influence the work reported in this paper.

Acknowledgments

This work has been supported by the Research Council of Finland through its Centres of Excellence Programme (2022-2029, LIBER) under project number. 346105 (M.L.) and 346111 (M.S.) and, Novo Nordisk Foundation under project nos. NNF20OC0061306 (M.L.), NNF22OC0079084 (A.S.) and NNF22OC0074060 (M.S.), as well as Research Council of Finland projects 352955 (I.T.) and 359180 (M.S.). We are grateful for the support by FinnCERES Materials Bioeconomy Ecosystem. Computational resources by CSC IT Centre for Finland, RAMI – RawMatters Finland, and Aalto University at OtaNano – Nanomicroscopy Center (Aalto-NMC). We acknowledge CSC for awarding this project access to the LUMI supercomputer, owned by the EuroHPC Joint Undertaking, hosted by CSC (Finland) and the LUMI consortium through a CSC project call. The authors are grateful to Aleksandra Tolmacheva for work on the graphic abstract for this article.

Appendix A. Supplementary data

Supplementary data to this article can be found online at https://doi.org/10.1016/j.ijbiomac.2025.147712.

Data availability

Data associated with the manuscript, including simulation input files, number data for the figures, and analysis scripts are available at https://doi.org/10.23729/fd-c73b4785-2396-3273-a566-e3929081ead3.

References

[1] J.E. Gagner, W. Kim, E.L. Chaikof, Designing protein-based biomaterials for medical applications, Acta Biomater. 10 (2014) 1542–1557.
[2] A. Solomonov, A. Kozell, U. Shimanovich, Designing multifunctional biomaterials via protein self-assembly, Angew. Chem. Int. Ed. Eng. 63 (2024) e202318365.
[3] P.J. Babu, L. Suamte, Applications of silk-based biomaterials in biomedicine and biotechnology, Eng. Regen. 5 (2024) 56–69.
[4] B. Kundu, N.E. Kurland, S. Bano, C. Patra, F.B. Engel, V.K. Yadavalli, S.C. Kundu, Silk proteins for biomedical applications: bioengineering perspectives, Prog. Polym. Sci. 39 (2014) 251–267.
[5] J. Liu, X. Ge, L. Liu, W. Xu, R. Shao, Challenges and opportunities of silk protein hydrogels in biomedical applications, Mater. Adv. 3 (2022) 2291–2308.
[6] P. Aramwit, T. Siritientong, T. Srichana, Potential applications of silk sericin, a natural protein from textile industry by-products, Waste Manag. Res. 30 (2012) 217–224.
[7] I. Kopyeva, R.P. Brady, C.A. DeForest, Light-based fabrication and 4D customization of hydrogel biomaterials, Nat. Rev. Bioeng. (2024) 1–22.
[8] Z. Chen, C. Du, S. Liu, J. Liu, Y. Yang, L. Dong, W. Zhao, W. Huang, Y. Lei, Progress in biomaterials inspired by the extracellular matrix, Giant (Oxf.) 19 (2024) 100323.
[9] Y. Zhang, Q. Zhao, J. Zhang, S. Wei, F. Tao, P. Yang, Bio-inspired adaptive and responsive protein-based materials, ChemPlusChem 89 (2024) e202400309.
[10] Y. Gu, L. Yu, J. Mou, D. Wu, P. Zhou, M. Xu, Mechanical properties and application analysis of spider silk bionic material, E-Polymers 20 (2020) 443–457.
[11] H. Liu, S.G. Wise, J. Rnjak-Kovacina, D.L. Kaplan, M.M.M. Bilek, A.S. Weiss, J. Fei, S. Bao, Biocompatibility of silk-tropoelastin protein polymers, Biomaterials 35 (2014) 5138–5147.

[12] L.S. Wray, X. Hu, J. Gallego, I. Georgakoudi, F.G. Omenetto, D. Schmidt, D. L. Kaplan, Effect of processing on silk-based biomaterials: reproducibility and biocompatibility, J Biomed Mater Res B Appl Biomater 99 (2011) 89–101.
[13] Y. Cao, B. Wang, Biodegradation of silk biomaterials, Int. J. Mol. Sci. 10 (2009) 1514–1524.
[14] C. Guo, C. Li, D.L. Kaplan, Enzymatic degradation of Bombyx mori silk materials: a review, Biomacromolecules 21 (2020) 1678–1686.
[15] X. Huang, G. Liu, X. Wang, New secrets of spider silk: exceptionally high thermal conductivity and its abnormal change under stretching, Adv. Mater. 24 (2012) 1482–1486.
[16] R.L. Strader, Y. Shmidov, A. Chilkoti, Encoding structure in intrinsically disordered protein biomaterials, Acc. Chem. Res. 57 (2024) 302–311.
[17] B. Wang, S.S. Patkar, K.L. Kiick, Application of thermoresponsive intrinsically disordered protein polymers in nanostructured and microstructured materials, Macromol. Biosci. 21 (2021) e2100129.
[18] J. Li, S. Li, J. Huang, A.Q. Khan, B. An, X. Zhou, Z. Liu, M. Zhu, Spider silk-inspired artificial fibers, Adv. Sci. 9 (2022) e2103965.
[19] J.L. Yarger, B.R. Cherry, A. van der Vaart, Uncovering the structure–function relationship in spider silk, Nat. Rev. Mater. 3 (2018) 18008.
[20] D. Fedorov, N. Roas-Escalona, D. Tolmachev, A.L. Harmat, A. Scacchi, M. Sammalkorpi, A.S. Aranko, M.B. Linder, Triblock proteins with weakly dimerizing terminal blocks and an intrinsically disordered region for rational design of condensate properties, Small 20 (13) (2024) e2306817.
[21] A. Seisto, A.S. Borisova, R. Pylkkänen, P. Mohammadi, Tailoring hydrophobicity and strength in spider silk-inspired coatings via thermal treatments, Comput. Struct. Biotechnol. J. 25 (2024) 177–185.
[22] G. Greco, B. Schmuck, V. Fazio, G. Puglisi, G. Florio, N.M. Pugno, L. Fambri, A. Rising, Temperature-induced effects on wet-spun artificial spider silk fibers, Adv. Funct. Mater. 35 (2025).
[23] F. Zhang, Nonclassical nucleation pathways in protein crystallization, J. Phys. Condens. Matter 29 (2017) 443002.
[24] D. Fedorov, F.-E. Sammalisto, A.L. Harmat, M. Ahlberg, S. Koskela, M.P. Haataja, A. Scacchi, M. Sammalkorpi, M.B. Linder, Metastable liquid–liquid phase separation and aging lead to strong processing path dependence in mini-spidroin solutions, Adv. Funct. Mater. 35 (2025) 2410421.
[25] K.M. Ruff, S. Roberts, A. Chilkoti, R.V. Pappu, Advances in understanding stimulus-responsive phase behavior of intrinsically disordered protein polymers, J. Mol. Biol. 430 (2018) 4619–4635.
[26] Y. Tang, S. Bera, Y. Yao, J. Zeng, Z. Lao, X. Dong, E. Gazit, G. Wei, Prediction and characterization of liquid-liquid phase separation of minimalistic peptides, Cell Rep. Phys. Sci. 2 (2021) 100579.
[27] J. McCarty, K.T. Delaney, S.P.O. Danielsen, G.H. Fredrickson, J.-E. Shea, Complete phase diagram for liquid-liquid phase separation of intrinsically disordered proteins, J. Phys. Chem. Lett. 10 (2019) 1644–1652.
[28] E.W. Martin, T. Mittag, Relationship of sequence and phase separation in protein low-complexity regions, Biochemistry 57 (2018) 2478–2487.
[29] R.V. Pappu, S.R. Cohen, F. Dar, M. Farag, M. Kar, Phase transitions of associative biomacromolecules, Chem. Rev. 123 (2023) 8945–8987.
[30] A. Stradner, P. Schurtenberger, Potential and limits of a colloid approach to protein solutions, Soft Matter 16 (2020) 307–323.
[31] M.A. Winnik, A. Yekta, Associative polymers in aqueous solution, Curr. Opin. Colloid Interface Sci. 2 (1997) 424–436.
[32] P. Mohanty, U. Kapoor, D. Sundaravadivelu Devarajan, T.M. Phan, A. Rizuan, J. Mittal, Principles governing the phase separation of multidomain proteins, Biochemistry 61 (2022) 2443–2455.
[33] P.J. Flory, Thermodynamics of high polymer solutions, J. Chem. Phys. 9 (1941) 660–661.
[34] M.L. Huggins, Solutions of long chain compounds, J. Chem. Phys. 9 (1941) 440.
[35] H.-X. Zhou, V. Nguemaha, K. Mazarakos, S. Qin, Why do disordered and structured proteins behave differently in phase separation? Trends Biochem. Sci. 43 (2018) 499–516.
[36] T.S. Harmon, A.S. Holehouse, M.K. Rosen, R.V. Pappu, Intrinsically disordered linkers determine the interplay between phase separation and gelation in multivalent proteins, Elife 6 (2017) e30294.
[37] S. Rekhi, D. Sundaravadivelu Devarajan, M.P. Howard, Y.C. Kim, A. Nikoubashman, J. Mittal, Role of strong localized vs weak distributed interactions in disordered protein phase separation, J. Phys. Chem. B 127 (2023) 3829–3838.
[38] S. Kumar, D. Saha, V.K. Aswal, Modifying interprotein interactions for controlling heat-induced protein gelation, Phys. Rev. Mater. 7 (2023) 015601.
[39] W.S. Gosal, S.B. Ross-Murphy, Globular protein gelation, Curr. Opin. Colloid Interface Sci. 5 (2000) 188–194.
[40] D. Huemmerich, C.W. Helsen, S. Quedzuweit, J. Oschmann, R. Rudolph, T. Scheibel, Primary structure elements of spider dragline silks and their contribution to protein solubility, Biochemistry 43 (2004) 13604–13612.
[41] J. Tormo, R. Lamed, A.J. Chirino, E. Morag, E.A. Bayer, Y. Shoham, T.A. Steitz, Crystal structure of a bacterial family-III cellulose-binding domain: a general mechanism for attachment to cellulose, EMBO J. 15 (1996) 5739–5751.
[42] D.J. Leahy, I. Aukhil, H.P. Erickson, 2.0 A crystal structure of a four-domain segment of human fibronectin encompassing the RGD loop and synergy region, Cell 84 (1996) 155–164.
[43] I. Tunn, G. Beaune, J. Tersteegen, T. Välisalmi, J.V.I. Timonen, F. Brochard-Wyart, M.B. Linder, Bursting of condensates, Commun. Phys. 7 (2024) 1–13.
[44] D. Stengel, M. Saric, H.R. Johnson, T. Schiller, J. Diehl, K. Chalek, D. Onofrei, T. Scheibel, G.P. Holland, Tyrosine's unique role in the hierarchical assembly of recombinant spider silk proteins: from spinning dope to fibers, Biomacromolecules 24 (2023) 1463–1474.
[45] J.H. Exler, D. Hümmerich, T. Scheibel, The amphiphilic properties of spider silks are important for spinning, Angew. Chem. Int. Ed. Eng. 46 (2007) 3559–3562.
[46] L. Lemetti, S.-P. Hirvonen, D. Fedorov, P. Batys, M. Sammalkorpi, H. Tenhu, M. B. Linder, A.S. Aranko, Molecular crowding facilitates assembly of spidroin-like proteins through phase separation, Eur. Polym. J. 112 (2019) 539–546.
[47] P. Mohammadi, A.S. Aranko, L. Lemetti, Z. Cenev, Q. Zhou, S. Virtanen, C. P. Landowski, M. Penttilä, W.J. Fischer, W. Wagermaier, M.B. Linder, Phase transitions as intermediate steps in the formation of molecularly engineered protein fibers, Commun. Biol. 1 (2018) 86.
[48] P. Mohammadi, C. Jonkergouw, G. Beaune, P. Engelhardt, A. Kamada, J.V. I. Timonen, T.P.J. Knowles, M. Penttila, M.B. Linder, Controllable coacervation of recombinantly produced spider silk protein using kosmotropic salts, J. Colloid Interface Sci. 560 (2020) 149–160.
[49] P. Batys, D. Fedorov, P. Mohammadi, L. Lemetti, M.B. Linder, M. Sammalkorpi, Self-assembly of silk-like protein into nanoscale bicontinuous networks under phase-separation conditions, Biomacromolecules 22 (2021) 690–700.
[50] D.A. Tolmachev, M. Malkamäki, M.B. Linder, M. Sammalkorpi, Spidroins under the influence of alcohol: effect of ethanol on secondary structure and molecular level solvation of silk-like proteins, Biomacromolecules 24 (2023) 5638–5653.
[51] L. Lemetti, A. Scacchi, Y. Yin, M. Shen, M.B. Linder, M. Sammalkorpi, A. S. Aranko, Liquid-liquid phase separation and assembly of silk-like proteins is dependent on the polymer length, Biomacromolecules 23 (2022) 3142–3153.
[52] T. Arndt, K. Jaudzems, O. Shilkova, J. Francis, M. Johansson, P.R. Laity, C. Sahin, U. Chatterjee, N. Kronqvist, E. Barajas-Ledesma, R. Kumar, G. Chen, R. Strömberg, A. Abelein, M. Langton, M. Landreh, A. Barth, C. Holland, J. Johansson, A. Rising, Spidroin N-terminal domain forms amyloid-like fibril based hydrogels and provides a protein immobilization platform, Nat. Commun. 13 (2022) 4695.
[53] S. Nagarkar, T. Nicolai, C. Chassenieux, A. Lele, Structure and gelation mechanism of silk hydrogels, Phys. Chem. Chem. Phys. 12 (2010) 3834–3844.
[54] H. Wang, Y. Zhang, H. Shao, X. Hu, A study on the flow stability of regenerated silk fibroin aqueous solution, Int. J. Biol. Macromol. 36 (2005) 66–70.
[55] Z.A. Haider, M. Arai, K. Hirabayashi, Mechanism of the gelation of fibroin solution, Biosci. Biotechnol. Biochem. 57 (1993) 1910–1912.
[56] L.M. De Leon Rodriguez, Y. Hemar, J. Cornish, M.A. Brimble, Structure-mechanical property correlations of hydrogel forming β-sheet peptides, Chem. Soc. Rev. 45 (2016) 4797–4824.
[57] U.-J. Kim, J. Park, C. Li, H.-J. Jin, R. Valluzzi, D.L. Kaplan, Structure and properties of silk hydrogels, Biomacromolecules 5 (2004) 786–792.
[58] A. Matsumoto, J. Chen, A.L. Collette, U.-J. Kim, G.H. Altman, P. Cebe, D. L. Kaplan, Mechanisms of silk fibroin sol-gel transitions, J. Phys. Chem. B 110 (2006) 21630–21638.
[59] M.O. Pacheco, E.L. Aikman, H.K. Bagnis, I.K. Gerzenshtein, T.D. Truong, W. L. Stoppel, Degumming time governs self-assembled silk fibroin hydrogel properties through molecular weight and amino acid composition, Biomacromolecules 26 (2025) 5069–5085.
[60] S.M. Kelly, T.J. Jess, N.C. Price, How to study proteins by circular dichroism, Biochim. Biophys. Acta 1751 (2005) 119–139.
[61] L. Wang, C. Brasnett, L. Borges-Araújo, P.C.T. Souza, S.J. Marrink, Martini3-IDP: improved Martini 3 force field for disordered proteins, Nat. Commun. 16 (2025) 2874.
[62] T.D. Loose, P.G. Sahrmann, T.S. Qu, G.A. Voth, Changing your Martini can still give you a hangover, J. Chem. Theory Comput. 20 (2024) 9190–9208.
[63] S. Ulrich, A. Glišović, T. Salditt, A. Zippelius, Diffraction from the beta-sheet crystallites in spider silk, Eur. Phys. J. E Soft Matter. 27 (2008) 229–242.
[64] Y.-H. Lin, H.S. Chan, Phase separation and single-chain compactness of charged disordered proteins are strongly correlated, Biophys. J. 112 (2017) 2043–2046.
[65] G.L. Dignon, W. Zheng, R.B. Best, Y.C. Kim, J. Mittal, Relation between single-molecule properties and phase behavior of intrinsically disordered proteins, Proc. Natl. Acad. Sci. U. S. A. 115 (2018) 9929–9934.
[66] T.I. Morozova, N.A. García, O. Matsarskaia, F. Roosen-Runge, J.-L. Barrat, Structural and dynamical properties of elastin-like peptides near their lower critical solution temperature, Biomacromolecules 24 (2023) 1912–1923.
[67] D.J. Bauer, L.S. Stelzl, A. Nikoubashman, Single-chain and condensed-state behavior of hnRNPA1 from molecular simulations, J. Chem. Phys. 157 (2022) 154903.
[68] H.-Y. Chou, A. Aksimentiev, Single-protein collapse determines phase equilibria of a biological condensate, J. Phys. Chem. Lett. 11 (2020) 4923–4929.
[69] X. Zeng, A.S. Holehouse, A. Chilkoti, T. Mittag, R.V. Pappu, Connecting coil-to-globule transitions to full phase diagrams for intrinsically disordered proteins, Biophys. J. 119 (2020) 402–418.
[70] D. Sundaravadivelu Devarajan, J. Wang, B. Szała-Mendyk, S. Rekhi, A. Nikoubashman, Y.C. Kim, J. Mittal, Sequence-dependent material properties of biomolecular condensates and their relation to dilute phase conformations, Nat. Commun. 15 (2024) 1912.
[71] D.S. Simmons, I.C. Sanchez, A model for a thermally induced polymer coil-to-globule transition, Macromolecules 41 (2008) 5885–5889.
[72] G. Raos, G. Allegra, Chain collapse and phase separation in poor-solvent polymer solutions: a unified molecular description, J. Chem. Phys. 104 (1996) 1626–1645.
[73] M.J. Abraham, T. Murtola, R. Schulz, S. Páll, J.C. Smith, B. Hess, E. Lindahl, GROMACS: high performance molecular simulations through multi-level parallelism from laptops to supercomputers, SoftwareX 1–2 (2015) 19–25.
[74] S. Páll, M.J. Abraham, C. Kutzner, B. Hess, E. Lindahl, Tackling exascale software challenges in molecular dynamics simulations with GROMACS, in: Solving

Software Challenges for Exascale, Springer International Publishing, 2015, pp. 3–27.
[75] D. Petrov, B. Zagrovic, Are current atomistic force fields accurate enough to study proteins in crowded environments? PLoS Comput. Biol. 10 (2014) e1003638.
[76] S. Piana, J.L. Klepeis, D.E. Shaw, Assessing the accuracy of physical models used in protein-folding simulations: quantitative evidence from long molecular dynamics simulations, Curr. Opin. Struct. Biol. 24 (2014) 98–105.
[77] P.S. Shabane, S. Izadi, A.V. Onufriev, General purpose water model can improve atomistic simulations of intrinsically disordered proteins, J. Chem. Theory Comput. 15 (2019) 2620–2634.
[78] J. Henriques, M. Skepö, Molecular dynamics simulations of intrinsically disordered proteins: on the accuracy of the TIP4P-D water model and the representativeness of protein disorder models, J. Chem. Theory Comput. 12 (2016) 3407–3415.
[79] R.B. Best, W. Zheng, J. Mittal, Balanced protein–water interactions improve properties of disordered proteins and non-specific protein association, J. Chem. Theory Comput. 10 (2014) 5113–5124.
[80] J.L.F. Abascal, C. Vega, A general purpose model for the condensed phases of water: TIP4P/2005, J. Chem. Phys. 123 (2005) 234505.
[81] T. Graen, R. Klement, A. Grupi, E. Haas, H. Grubmüller, Transient secondary and tertiary structure formation kinetics in the intrinsically disordered state of α-synuclein from atomistic simulations, Chemphyschem 19 (2018) 2507–2511.
[82] D. Fedorov, P. Batys, D.B. Hayes, M. Sammalkorpi, M.B. Linder, Analyzing the weak dimerization of a cellulose binding module by analytical ultracentrifugation, Int. J. Biol. Macromol. 163 (2020) 1995–2004.
[83] S. Nosé, A unified formulation of the constant temperature molecular dynamics methods, J. Chem. Phys. 81 (1984) 511–519.
[84] W.G. Hoover, Canonical dynamics: equilibrium phase-space distributions, Phys. Rev. A Gen. Phys. 31 (1985) 1695–1697.
[85] M. Parrinello, A. Rahman, Polymorphic transitions in single crystals: a new molecular dynamics method, J. Appl. Phys. 52 (1981) 7182–7190.
[86] T. Darden, D. York, L. Pedersen, Particle mesh Ewald: an N·log(N) method for Ewald sums in large systems, J. Chem. Phys. 98 (1993) 10089–10092.
[87] U. Essmann, L. Perera, M.L. Berkowitz, T. Darden, H. Lee, L.G. Pedersen, A smooth particle mesh Ewald method, J. Chem. Phys. 103 (1995) 8577–8593.
[88] B. Hess, P-LINCS: a parallel linear constraint solver for molecular simulation, J. Chem. Theory Comput. 4 (2008) 116–122.
[89] R. Gowers, M. Linke, J. Barnoud, T. Reddy, M. Melo, S. Seyler, J. Domański, D. Dotson, S. Buchoux, I. Kenney, O. Beckstein, MDAnalysis: a python package for the rapid analysis of molecular dynamics simulations, in: Proceedings of the 15th Python in Science Conference, SciPy, 2016.
[90] N. Michaud-Agrawal, E.J. Denning, T.B. Woolf, O. Beckstein, MDAnalysis: a toolkit for the analysis of molecular dynamics simulations, J. Comput. Chem. 32 (2011) 2319–2327.
[91] W. Humphrey, A. Dalke, K. Schulten, VMD: visual molecular dynamics, J. Mol. Graph. 14 (33–8) (1996) 27–28.
[92] A. Krishnan, A. Giuliani, J.P. Zbilut, M. Tomita, Implications from a network-based topological analysis of ubiquitin unfolding simulations, PLoS One 3 (2008) e2149.
[93] E. Papaleo, P. Mereghetti, P. Fantucci, R. Grandori, L. De Gioia, Free-energy landscape, principal component analysis, and structural clustering to identify representative conformations from molecular dynamics simulations: the myoglobin case, J. Mol. Graph. Model. 27 (2009) 889–899.
[94] S.M. Bhattacharjee, A. Giacometti, A. Maritan, Flory theory for polymers, J. Phys. Condens. Matter 25 (2013) 503101.
[95] N.H. Williamson, M. Röding, S.J. Miklavcic, M. Nydén, Scaling exponent and dispersity of polymers in solution by diffusion NMR, J. Colloid Interface Sci. 493 (2017) 393–397.
[96] M. Rubinsten, R. Colby H, Polymer Physics, Oxford University Press, Oxford, England, 2003.
[97] H. Hofmann, A. Soranno, A. Borgia, K. Gast, D. Nettels, B. Schuler, Polymer scaling laws of unfolded and intrinsically disordered proteins quantified with single-molecule spectroscopy, Proc. Natl. Acad. Sci. U. S. A. 109 (2012) 16155–16160.
[98] Y.-H. Lin, J.P. Brady, J.D. Forman-Kay, H.S. Chan, Charge pattern matching as a 'fuzzy' mode of molecular recognition for the functional phase separations of intrinsically disordered proteins, New J. Phys. 19 (2017) 115003.
[99] J.A. Riback, C.D. Katanski, J.L. Kear-Scott, E.V. Pilipenko, A.E. Rojek, T. R. Sosnick, D.A. Drummond, Stress-triggered phase separation is an adaptive, evolutionarily tuned response, Cell 168 (2017) 1028–1040.e19.
[100] J. Wang, D. Sundaravadivelu Devarajan, K. Muthukumar, Y.C. Kim, A. Nikoubashman, J. Mittal, Sequence-dependent conformational transitions of disordered proteins during condensation, Chem. Sci. 15 (2024) 20056–20063.
[101] D. Karandur, K.-Y. Wong, B.M. Pettitt, Solubility and aggregation of Gly(5) in water, J. Phys. Chem. B 118 (2014) 9565–9572.
[102] M. Auton, D.W. Bolen, Additive transfer free energies of the peptide backbone unit that are independent of the model compound and the choice of concentration scale, Biochemistry 43 (2004) 1329–1342.
[103] S. Rauscher, V. Gapsys, M.J. Gajda, M. Zweckstetter, B.L. de Groot, H. Grubmüller, Structural ensembles of intrinsically disordered proteins depend strongly on force field: a comparison to experiment, J. Chem. Theory Comput. 11 (2015) 5513–5524.
[104] P. Robustelli, S. Piana, D.E. Shaw, Developing a molecular dynamics force field for both folded and disordered protein states, Proc. Natl. Acad. Sci. U. S. A. 115 (2018) E4758–E4766.
[105] N.K. Li, F. García Quiroz, C.K. Hall, A. Chilkoti, Y.G. Yingling, Molecular description of the LCST behavior of an elastin-like polypeptide, Biomacromolecules 15 (2014) 3522–3530.
[106] D. López Barreiro, I.J. Minten, J.C. Thies, C.M.J. Sagt, Structure-property relationships of elastin-like polypeptides: a review of experimental and computational studies, ACS Biomater Sci. Eng. 9 (2023) 3796–3809.
[107] B. Zhao, N.K. Li, Y.G. Yingling, C.K. Hall, LCST behavior is manifested in a single molecule: elastin-like polypeptide (VPGVG)n, Biomacromolecules 17 (2016) 111–118.
[108] A. Leppert, G. Chen, D. Lama, C. Sahin, V. Railaite, O. Shilkova, T. Arndt, E. G. Marklund, D.P. Lane, A. Rising, M. Landreh, Liquid-liquid phase separation primes spider silk proteins for fiber formation via a conditional sticker domain, Nano Lett. 23 (2023) 5836–5841.
[109] M. Landreh, H. Osterholz, G. Chen, S.D. Knight, A. Rising, A. Leppert, Liquid-liquid crystalline phase separation of spider silk proteins, Commun. Chem. 7 (2024) 260.
[110] G. Greco, T. Arndt, B. Schmuck, J. Francis, F.G. Bäcklund, O. Shilkova, A. Barth, N. Gonska, G. Seisenbaeva, V. Kessler, J. Johansson, N.M. Pugno, A. Rising, Tyrosine residues mediate supercontraction in biomimetic spider silk, Commun. Mater. 2 (2021) 1–10.
[111] C.-F. Hu, C.-Y. Gan, Y.-J. Zhu, X.-X. Xia, Z.-G. Qian, Modulating polyalanine motifs of synthetic spidroin for controllable preassembly and strong fiber formation, ACS Biomater Sci. Eng. 10 (2024) 2925–2934.
[112] I. Levy, O. Shoseyov, Cellulose-binding domains: biotechnological applications, Biotechnol. Adv. 20 (2002) 191–213.
[113] M. Jackson, H.H. Mantsch, The use and misuse of FTIR spectroscopy in the determination of protein structure, Crit. Rev. Biochem. Mol. Biol. 30 (1995) 95–120.
[114] X. Hu, D. Kaplan, P. Cebe, Determining beta-sheet crystallinity in fibrous proteins by thermal analysis and infrared spectroscopy, Macromolecules 39 (2006) 6161–6170.
[115] N. Greenfield, G.D. Fasman, Computed circular dichroism spectra for the evaluation of protein conformation, Biochemistry 8 (1969) 4108–4116.
[116] E. Pauthe, J. Pelta, S. Patel, D. Lairez, F. Goubard, Temperature-induced β-aggregation of fibronectin in aqueous solution, Biochim. Biophys. Acta 1597 (2002) 12–21.
[117] S.V. Litvinovich, K.C. Ingham, Interactions between type III domains in the 110 kDa cell-binding fragment of fibronectin, J. Mol. Biol. 248 (1995) 611–626.
[118] A. Kulshrestha, S.N. Punnathanam, K.G. Ayappa, Finite temperature string method with umbrella sampling using path collective variables: application to secondary structure change in a protein, Soft Matter 18 (2022) 7593–7603.
[119] M. Vanhalle, S. Corneillie, M. Smet, P. Van Puyvelde, B. Goderis, Poly(alanine): structure and stability of the D and L-enantiomers, Biomacromolecules 17 (2016) 183–191.
[120] K.A. Henzler Wildman, D.-K. Lee, A. Ramamoorthy, Determination of alpha-helix and beta-sheet stability in the solid state: a solid-state NMR investigation of poly (L-alanine), Biopolymers 64 (2002) 246–254.
[121] D. Su, M. Yao, J. Liu, Y. Zhong, X. Chen, Z. Shao, Enhancing mechanical properties of silk fibroin hydrogel through restricting the growth of β-sheet domains, ACS Appl. Mater. Interfaces 9 (2017) 17489–17498.
[122] K. Yazawa, K. Ishida, H. Masunaga, T. Hikima, K. Numata, Influence of water content on the β-sheet formation, thermal stability, water removal, and mechanical properties of silk materials, Biomacromolecules 17 (2016) 1057–1066.
[123] E.S. Gil, R.J. Spontak, S.M. Hudson, Effect of beta-sheet crystals on the thermal and rheological behavior of protein-based hydrogels derived from gelatin and silk fibroin, Macromol. Biosci. 5 (2005) 702–709.
[124] Y. Hu, Q. Zhang, R. You, L. Wang, M. Li, The relationship between secondary structure and biodegradation behavior of silk fibroin scaffolds, Adv. Mater. Sci. Eng. 2012 (2012).
[125] Y. Kambe, Y. Mizoguchi, K. Kuwahara, T. Nakaoki, Y. Hirano, T. Yamaoka, Beta-sheet content significantly correlates with the biodegradation time of silk fibroin hydrogels showing a wide range of compressive modulus, Polym. Degrad. Stab. 179 (2020) 109240.
[126] A.S. Borisova, T. Virkkala, R. Pylkkänen, M. Kellock, P. Mohammadi, Toughening brittle kraft lignin coating on mismatched substrate with spider silk-inspired protein as an interfacial modulator, J. Colloid Interface Sci. 655 (2024) 789–799.
[127] A. Brodkorb, T. Croguennec, S. Bouhallab, J.J. Kehoe, Heat-induced denaturation, aggregation and gelation of whey proteins, in: P.L.H. McSweeney, J.A. O'Mahony (Eds.), Advanced Dairy Chemistry: Volume 1B: Proteins: Applied Aspects, Springer New York, New York, NY, 2016, pp. 155–178.
[128] T. Mittag, R.V. Pappu, A conceptual framework for understanding phase separation and addressing open questions and challenges, Mol. Cell 82 (2022) 2201–2214.
[129] M.C. Cohan, R.V. Pappu, Making the case for disordered proteins and biomolecular condensates in bacteria, Trends Biochem. Sci. 45 (2020) 668–680.
[130] D. Mangal, S. Jamali, Role of interaction range on the microstructure and dynamics of attractive colloidal systems, Soft Matter 20 (2024) 4466–4473.
[131] A.L. Bug, S.A. Safran, G.S. Grest, I. Webman I., Do interactions raise or lower a percolation threshold? Phys. Rev. Lett. 55 (1985) 1896–1899.
[132] G. Wang, J.W. Swan, Surface heterogeneity affects percolation and gelation of colloids: dynamic simulations with random patchy spheres, Soft Matter 15 (2019) 5094–5108.
[133] P. Atkins, J. de Paula, J. Keeler, Atkins' Physical Chemistry, Oxford University Press, 2022.

[134] J.J. McManus, P. Charbonneau, E. Zaccarelli, N. Asherie, The physics of protein self-assembly, Curr. Opin. Colloid Interface Sci. 22 (2016) 73–79.
[135] P.G. de Gennes, Scaling Concepts in Polymer Physics, Cornell University Press, Ithaca, NY, 1979.
[136] P.G. de Gennes, Reptation of a polymer chain in the presence of fixed obstacles, in: Series on Directions in Condensed Matter Physics, World Scientific Publishing Company, 2009, pp. 35–42.